Spleen-derived Small Extracellular Vesicles Protect against Myocardial Infarction via Mediating Spleen-heart Crosstalk

Keyu Liu[1,*], MD, Yue Luo[1,*], MD, Weifeng Liao[2,3.*], MD, Riken Chen[4,*], MD, PhD, Tugang Chen[5], MD, PhD, Haitao Huang[5], MD, Jinrong Xu[5], MD, Fang Fang[6], PhD, Qinghua Chen[2], Dongling Lin[2], Ting Gu[2], Burton B Yang[7,#], MD, PhD, Wenliang Chen[2,3,#], MD, PhD, Liangqing Zhang[1,#], MD, PhD.

1 Department of Anesthesiology, the Second Affiliated Hospital of Guangdong Medical University, Guangdong Medical University, Zhanjiang, Guangdong, China

2 Translational Medicine Center, the Second Affiliated Hospital of Guangdong Medical University, Guangdong Medical University, Zhanjiang, Guangdong, China

3 Medical Interdisciplinary Science Research Center of Western Guangdong, the Second Affiliated Hospital of Guangdong Medical University, Guangdong Medical University, Zhanjiang, Guangdong, China

4 Respiratory and Critical Care Medicine, the Second Affiliated Hospital of Guangdong Medical University, Zhanjiang, Guangdong, China

5 Department of Cardiovascular Medicine, the Second Affiliated Hospital of Guangdong Medical University, Guangdong Medical University, Zhanjiang, Guangdong, China

6 Office of Academic Research, the Second Affiliated Hospital of Guangdong Medical University, Guangdong Medical University, Zhanjiang, Guangdong, China

7 Department of Laboratory Medicine and Pathobiology, University of Toronto, 2075 Bayview Ave, Toronto, Ontario, M4N 3M5 Canada

Short title: A novel mediator in cardiosplenic axis

* These authors contribute equally.

Correspondence:

Liangqing Zhang, email: zhangliangqing@gdmu.edu.cn, Department of Anesthesiology, the Second Affiliated Hospital of Guangdong Medical University, Guangdong Medical University, Zhanjiang, Guangdong, China

Wenliang Chen, email: chenwl@gdmu.edu.cn, Translational Medicine Center, the Second Affiliated Hospital of Guangdong Medical University, Guangdong Medical University, Zhanjiang, Guangdong, China

Burton B Yang, email: byang@sri.utoronto.ca, Department of Laboratory Medicine and Pathobiology, University of Toronto, 2075 Bayview Ave, Toronto, Ontario, M4N 3M5 Canada

Words count：10238 words

Abstract

Background: The cardiosplenic axis has recently begun to be recognized as an important mediator in ischemic heart disease, but its mechanistic role remains incompletely understood. This study aimed to investigate novel molecular mechanisms underlying spleen-heart crosstalk in acute myocardial infarction (AMI), focusing on the role of spleen-derived small extracellular vesicles (sEVs).

Methods: We used both a murine AMI model and an oxygen-glucose deprivation (OGD) cell model. Orthogonal approaches, including splenectomy, TTC staining, Masson's trichrome staining, wheat agglutinin staining, echocardiography, TUNEL staining, RNA sequencing, transmission electron microscope imaging, GW4869 administration as a sEVs inhibitor, and functional assays, was employed to evaluate the role of spleen-derived sEVs in AMI-induced cardiac injuries and dysfunction. 4D-proteomics was conducted to profile the protein cargo of sEVs. The function of mitochondrial pyruvate carrier 1 (MPC1) was evaluated with specific antibody blockade and pharmacological inhibition (UK5099, GW604714x). Plasma levels of sEVs-capsulated MPC1 were compared between patients with and without coronary heart disease (CHD), and AMI using ELISA.

Results: Spleen immune activity was upregulated in AMI mice. Splenectomy worsened AMI outcomes by reducing survival, impairing cardiac function, and increasing fibrosis. Spleen-derived sEVs levels increased with a temporal manner following AMI and was taken up by ischemic myocardium, peaking at day 3 post AMI (defined as M3D-sEVs). Administration of M3D-sEVs improved survival, reduced

infarct size, and restored mitochondrial respiration. Conversely, sEVs depletion by GW4869 aggravated cardiac ischemic damage and left ventricle dysfunction. Proteomic analysis revealed that cardioprotective M3D-sEVs were enriched for MPC1, which promoted pyruvate metabolism and increased ATP/ADP ratio in recipient cardiomyocytes. Neutralization of MPC1 within M3D-sEVs abrogated these beneficial effects. Clinically, plasma sEVs-MPC1 levels were significantly elevated in AMI patients compared to CHD patients without AMI, and in CHD patients compared to non-CHD controls.

Conclusions: The spleen exerts cardioprotection against AMI by releasing MPC1-enriched sEVs that preserve mitochondrial energetics in the injured myocardium. Augmenting this endogenous sEVs-mediated pathway may represent a promising therapeutic strategy for ischemic cardiomyopathy.

Keywords: Acute myocardial infarction; Spleen; Small extracellular vesicles; MPC1; Cardiosplenic axis

Clinical Perspective

What Is New?

- Acute myocardial infarction (AMI) induces transcriptional activation of splenic extracellular vesicle-related genes, resulting in elevated vesicle secretion.
- Following AMI, splenic sEVs enriched with mitochondrial pyruvate carrier 1 (MPC1) increase in response to cardiac injury. These sEVs enhance mitochondrial metabolic energy production in the heart, critically influencing post-MI outcomes, displaying as reducing mortality, promoting wound healing and repair, and attenuating long-term adverse cardiac remodeling.
- Levels of MPC1 in circulating sEVs are elevated in patients with coronary heart disease (CHD) and show a further significant increase in those with AMI patients.

What Are the Clinical Implication?

- Our findings reveal a novel heart-spleen communication axis mediated by sEVs following AMI. These vesicular messengers enhance cardiac mitochondrial energy metabolism in the injured myocardium, ultimately improving functional recovery and clinical outcomes post-MI.
- Circulating sEVs MPC1 is a potential biomarker for the diagnosis of myocardial injury.

Abbreviations

CVD, Cardiovascular Disease. **CHD,** Coronary Heart Disease. **AMI,** Acute myocardial infarction. **OGD,** Oxygen-glucose deprivation. **sEVs,** Small extracellular vesicles. **P-sEVs,** Plasma small extracellular vesicles. **AARIVE,** Animal Research: Reporting of In vivo Experiments. **Echo,** Echocardiograph. **EF,** ejection fraction. **FS,** fractional shortening. **MPC1,** Mitochondrial pyruvate carrier 1. **PCK2,** Phosphoenolpyruvate carboxykinase 2. **α-SMA,** α-smooth muscle actin. **Bax,** Bcl-2-associated X protein. **TUNEL,** terminal deoxynucleotidyl transferase dUTP nick end labeling. **C-Cas-3,** cleaved caspase 3. **CK-MB,** creatine kinase MB isoenzyme. **ELISA,** Enzyme-Linked Immunosorbent Assay. **WGA,** Wheat germ agglutinin. **nFCM,** Nano-flow cytometer. **OCR,** Oxygen Consumption Rate. **LC-MS**, Liquid Chromatograph Mass Spectrometer.

RNA-seq, RNA sequencing. **LV,** left ventricular. ETC, Electron Transport Chain. **TCA,**

Tricarboxylic Acid. **4D-DIA,** Four-dimensional data-independent acquisition.

130

131

Introduction

Acute myocardial infarction (AMI) results from sudden interruption of coronary blood flow, leading to ischemia and subsequent injury to the myocardium. Despite major advancements in early reperfusion therapy, AMI remains a leading cause of morbidity and mortality worldwide[1]. A deeper understanding of the molecular mechanisms involved in AMI pathogenesis and an identification of novel therapeutic targets are still urgently needed.

The concept of crosstalk between the spleen and heart, termed the cardiosplenic axis, was first described in 1949 that splenic nerves activation by electric stimulation improves ventricle function in dogs[2]. Since then, the spleen has been implicated cardioprotection, potentially through its regulation of inflammatory processes after myocardial injury by mobilizing immune cell populations such as monocytes and by releasing signaling factors that influence downstream effects within the heart[3,4]. For example, stimulation of splenic activity vie the vagus nerve during remote ischemic conditioning was shown to reduce cardiac infarct size in a rat model of AMI[5], suggesting that spleen-derived factors may play a critical role in modulating ischemic cardiac injury. However, the precise molecular mechanisms underlying heart-spleen communication remain to be fully elucidated.

Small extracellular vesicles (sEVs), including exosomes, have be proposed as critical mediators of intercellular and inter-organ signaling[6], particularly in the context of cardiovascular injury[7]. sEVs are nanosized vesicles (30-150nm) that carry a diverse range of bioactive molecular cargo, including proteins, lipids, and nucleic acids. The

cargos are shuttled systemically to recipient cells to regulate their function. The roles of sEVs in mediating cellular and organ-level communications make it promising candidates for use as disease biomarkers, therapeutic agents, or drug delivery vehivles[8]. Recent studies have shown that plasma sEVs derived from AMI patients promote angiogenesis, regulate ferroptosis and autophagy, and thus to alleviate hypoxic myocardial injuries[9-11]. It has also been reported that the majority of plasma sEVs in AMI patients originate from the spleen[12], indicating that spleen-derived sEVs play critical roles in the pathophysiology of AMI.

Ischemic injury triggers a cascade of pathological responses, including inflammation, metabolic dysfunction, and cell death, which ultimately contribute to adverse cardiac remodeling and progression to heart failure[13]. Among these processes, mitochondrial dysfunction plays a central role in AMI, as the heart's high energy demands are heavily dependent on mitochondrial oxidative metabolism[14]. Ischemia-induced impairment of mitochondrial function compromises ATP production generates excessive reactive oxygen species (ROS), and promotes cardiomyocyte apoptosis, further exacerbating myocardial injury and impairing functional recovery[15]. Mitochondrial Pyruvate Carrier 1 (MPC1), a key subunit of the mitochondrial pyruvate carrier (MPC) complex, has gained attention as a critical regulator of mitochondrial bioenergetics. The MPC complex, composed of MPC1 and MPC2, facilitates transport of pyruvate from the cytosol into the mitochondrial matrix, enabling its subsequent entry into the tricarboxylic acid (TCA) cycle and oxidative phosphorylation[16]. Pyruvate metabolism is essential for efficient energy production,

particularly in cardiomyocytes, which has a limited capacity to adapt to metabolic stress[17]. Dysregulation of MPC1 expression or function in ischemic conditions disrupts this process, leading to cytosolic pyruvate accumulation, diminished TCA cycle activity, and a shift toward less efficient anaerobic glycolysis[18]. Restoration of MPC1 expression during ischemic injury has been shown to enhance mitochondrial function, reduce oxidative stress, and facilitate cardiomyocyte survival, making MPC1 as a promising therapeutic target for metabolic management of AMI[19].

In this study, we investigated the crosstalk between spleen and heart during AMI, focusing on the potential role of spleen-derived sEVs in delivering MPC1 to the ischemic heart and preserving mitochondrial function in cardiomyocytes. Elucidating these mechanisms may offer valuable insights into systemic regulation of mitochondrial bioenergetics and identify novel therapeutic strategies to enhance myocardial repair and recovery following ischemic injury.

Methods

Detailed methods

Comprehensive descriptions of experimental procedures, protocols, and reagents are provided in the Supplemental Material.

Data Availability Statement

The data, analytic methods, and study materials supporting the findings of this study are available to other researchers from the corresponding author upon reasonable request. RNA sequencing (RNA-seq) raw data have been deposited at the National

Center for Biotechnology Information (BioProject: PRJNA1262715). Mass spectrometry proteomics data have been deposited to the Proteome Xchange Consortium (https://proteomecentral.proteomexchange.org) with the dataset identifier PXD064000 and PXD063946.

Study Participants

A total of 128 subjects undergoing evaluation for coronary artery disease were enrolled in this study. Among these, 104 patients scheduled for coronary angiography were included, being composed of 21 patients with coronary heart disease (CHD) and myocardial infarction (MI), 48 patients with CHD without MI, and 35 patients without CHD. Plasma and plasma sEVs MPC1 levels were measured in all participants. Written informed consent was obtained from all subjects, and the study protocol was approved by the Human Ethics Committee of the Second Affiliated Hospital of Guangdong Medical University (No. PJKT2024-163), in accordance with the ethical guidelines of the 1975 Declaration of Helsinki.

Animal Experiments

Male C57BL/6 mice (6-8 weeks old, 20-25 g) were purchased from Guangzhou Tengke Biomedical Technology Co., Ltd (Guangzhou, China). Mice were housed under specific pathogen free conditions at 25 ± 2 °C with a 12 h light/dark cycle and ad libitum access to food and water. MI surgery was performed in 8- to 10-week-old mice by permanent ligation of the left anterior descending coronary artery (LAD). All animal protocols were approved by the Guangdong Medical University Animal Care and Use Committee (GDMU-2024-000043) and conducted in accordance with the

ARRIVE 2.0 (Animal Research Reporting of In Vivo Experiments) guidelines.

Statistical Analysis

For in vitro and in vivo experiments, cells or animals were randomly assigned to experimental groups. At least five biologically independent replicates were performed per group. Data are presented as mean ± standard error of the mean (SEM) for normally distributed variables, or as median (interquartile range) as appropriate. Normality was assessed using the Shapiro-Wilk test. For normally distributed data, comparisons between two groups were performed using unpaired two-tailed Student's t test, and comparisons among more than two groups were performed using one-way ANOVA with Tukey's or Dunn's multiple comparisons test as appropriate. For non-normally distributed data, the Mann-Whitney U test (two groups) or Kruskal-Wallis test with Dunn's post-hoc test (>2 groups) was used. When two independent factors were analyzed, two-way ANOVA with Tukey's multiple comparisons test was applied. Mixed-effects ANOVA was used for serial echocardiographic measurements. Homogeneity of variance was tested with the Brown-Forsythe test; if violated, the Welch test was used. Survival analyses were performed using the Kaplan-Meier method and log-rank test. Statistical analyses were conducted using GraphPad Prism (version 9.0). Significance was defined as $P < 0.05$.

For clinical data, categorical variables are reported as counts and percentages, with comparisons performed using Chi-square or Fisher's exact tests as appropriate. All statistical tests were two-sided, with significance set at $P < 0.05$. Clinical statistical

analyses were performed using SPSS (version 27.0, IBM). Detailed statistical approaches and replicate numbers are provided in the figure legends.

Results

Splenectomy aggravates cardiac injury in AMI mice

We first assessed the splenic immune response post myocardial ischemia in AMI mice. As expected, both heart and spleen weights were significantly increased in AMI mice compared to sham-operated controls on day 3 post AMI (Figure S1A-S1C). The white pulp, which is critical for the initiation of adaptive immune responses in spleen[20,21], was significantly enlarged in AMI mice, as demonstrated by H&E staining; the marginal zone was also expanded relative to sham mice (Figure S1D-S1F). In the meantime, mRNA expression of inflammatory cytokines, such as IL-6, IFN-γ, TNF-α, IL-10, was significantly upregulated in the spleens of AMI mice, with all cytokines peaking at day 3 post AMI (Figure S1G-S1J). These findings indicate that splenic biological activity is markedly enhanced in response to myocardial ischemic injury.

Previous studies have reported variable effects of splenectomy on cardiac injury[22-24]. To clarify the impact of spleen removal, we performed splenectomy immediately following ligation of left anterior descending (LAD) of coronary artery in AMI mice and evaluated cardiac outcomes. Compared with AMI mice with intact spleens, splenectomized AMI mice exhibited significantly poorer survival rates, reduced left ventricular ejection fraction and fractional shortening (Figure 1A-1D), larger cardiac infarct size (Figure 1E-1F), and higher serum creatine kinase-MB (CK-MB) levels

(Figure S2A). Splenectomy also led to a dramatical increase in cardiac collagen deposition, as determined by Masson's trichrome staining (Figure 1G-1H), and elevated expression of fibrosis-related proteins, such as α smooth muscle actin (α-SMA), collagen I (Col), and fibronectin (FN), in MI hearts (Figure 1I-1J), indicating that splenectomy increased cardiac fibrosis post AMI. Furthermore, splenectomized mice also exhibited a higher proportion of TUNEL positive cardiomyocytes (Figure 1K-1L), increased expression of pro-apoptotic markers Bax and cleaved caspase-3 (C-Cas3) and decreased expression of anti-apoptotic protein Bcl2 expression in heart at day 3 post AMI (Figure 1M-1N). Myocardial hypertrophic remodeling, as measured by wheat germ agglutinin (WGA) staining at 28 days post MI, was also significantly aggravated in splenectomized AMI mice compared to controls (Figure 1O-1P). Histological analyses revealed that splenectomy with AMI mice worsened myocardial structural disarray, as shown by H&E staining (Figure S2B). These results together demonstrate that splenectomy significantly worsens cardiac dysfunction and adverse remodeling following AMI, indicating the existence of spleen-heart crosstalk and supporting an endogenously protective role of the spleen against ischemic cardiac injury.

Extracellular vesicles-related gene expression is upregulated in the spleen of AMI mice

To investigate transcriptomics alteration in the spleen post AMI, we performed RNA-Seq analysis of spleen tissues (Figure 2A). A total of 2621 differentially

expressed genes (DEGs) were found in spleens from AMI mice versus sham-operated controls, with 1129 genes upregulated and 1492 genes downregulated (Figure 2B and Figure S3A). Gene Ontology (GO) analysis revealed that these DEGs were predominantly enriched in biological function associated with extracellular vesicles (Figure S3B-S3E). Gene set enrichment analysis (GSEA) further demonstrated a significant increase in gene signatures related to extracellular exosome and vesicle regulation in the MI group compared with the sham group (Figure S3F-S3G). The biogenesis processes of EVs are intricate and can be affected by multiple pathways[25], such as soluble N-ethylmaleimide-sensitive fusion attachment protein receptor (SNARE), Neutral sphingomyelin phosphodiesterase 3 (Smpd3), and Rab GTPases (e.g., Rab27a/Rab27b, Rab11). Therefore, we sought to validate RNA-Seq findings by assessing the expression levels of key sEVs biogenesis-related genes via quantitative PCR. Several genes involved in sEVs formation and trafficking, including Rab27a, Rab31, Rab11, Pdcd6ip, Rab22a, and Smpd3, were found to be significantly upregulated in the spleens of AMI mice compared to sham controls (Figure 2C), which is consistent with RNA-Seq results. These findings indicate that myocardial ischemia induces the upregulation of extracellular vesicles biogenesis in the spleen, prompting further investigation into the role and function of spleen-derived sEVs in AMI.

Spleen-derived small extracellular vesicles biogenesis is enhanced in response to AMI

sEVs were isolated from mouse spleen using established protocols from our previous work[26] (Figure 2D). The physical characteristics of the isolated sEVs were validated by transmission electron microscopy (TEM), western blotting, and nano-flow cytometry (nFCM). The isolated particles were positive for conventional sEVs markers (TSG101, CD63, and CD9), while the negative markers GM130 and TBP were undetectable, confirming the purity of the preparations. We observed that both the protein contents and total particle number of spleen-derived sEVs were significantly increased in response to myocardial infarction (MI), peaking at day 3 post MI (Figure 2E-2F, Figure S4A). TEM and nFCM analysis showed that vesicles exhibited the expected cup-shaped, double-membrane morphology with diameters primarily ranging from 30 to 200 nm (Figure 2G-2H). These results confirm that the isolated particles are sEVs and indicate that splenic sEVs secretion is significantly increased during AMI, particularly peaking at day 3 post MI.

To determine if spleen-derived sEVs could reside in cardiac tissue in vivo, we labeled isolated spleen-derived sEVs with Dimethyl red dye (DIR dye) and administered them intramyocardially to mice. Bioluminescence imaging results showed that DIR-labeled sEVs isolated from the spleens of MI mice predominantly accumulated in the hearts of recipient AMI mice post injection (Figure 2I-2J), while markedly weak bioluminescence signals were observed in the liver, spleen, and lungs (Figure S4B), suggesting that spleen-derived sEVs preferentially target the ischemic myocardium. These findings demonstrate that biogenesis and release of spleen-derived sEVs are significantly upregulated during the acute phase of MI and that these vesicles are

capable of trafficking to the injured myocardium and accumulating within it.

Spleen-derived sEVs alleviate ischemic injuries in the heart and cardiomyocytes

We next evaluated the effects of spleen-derived sEVs on ischemic injury induced by AMI. Recipient AMI mice received intramyocardial injections of spleen-derived sEVs isolated from donor sham or AMI mice. Comparative analyses revealed that M3D-sEVs exerted the most predominant beneficial effects on survival in recipient AMI mice, significantly increasing survival rates compared to other groups (Figure 3A). In addition, M3D-sEVs but not M1D-sEVs or M7D-sEVs administration markedly improve cardiac function, as evidenced by significantly increased left ventricular ejection fraction and fractional shortening (Figure 3B-3D), reduced infarct area (Figure 3E-3F) and decreased collagen accumulation (Figure 3G and 3H) in recipient AMI mice. Furthermore, M3D-sEVs significantly attenuated the expression of fibrosis-related proteins (α-SMA, Col, and FN) (Figure 3I and 3J) in hearts of recipient AMI mice. M3D-sEVs treatment led to decreased myocardial structural disarray, TUNEL-positive cardiomyocytes, and serum CK-MB levels (Figure S5A-S5D). It also modulated apoptosis-related protein expression, with downregulation of Bax and cleaved caspase-3 (C-Cas-3), and upregulation of Bcl2 (Figure 3K-3L). Additionally, M3D-sEVs alleviated cardiac hypertrophy in ischemic mouse hearts (Figure 3M-3N).

To further investigate the direct effects on cardiomyocytes, H9C2 cells were incubated with PKH26-labeled M3D-sEVs. Fluorescent signal was readily observed within H9C2 cells at 12 and 24 hours post treatment (Figure S6A), suggesting

efficient sEVs uptake by these cells. Consistent with the in vivo findings, M3D-sEVs treatment affected expressions of apoptosis-related proteins in H9C2 cells subjected to OGD, resulting in upregulation of Bcl2 and downregulation of C-Cas-3 and Bax (Figure S6B-S6C).

Taken together, these results demonstrate that spleen-derived sEVs, specifically those collected at day 3 post AMI, exert significant cardioprotective effects by attenuating ischemic injury and apoptosis both in vivo and in vitro. Accordingly, M3D-sEVs were used in subsequent experiments.

Blockage of sEVs biogenesis aggravated cardiac ischemic injury in mice

To further assess the functional importance of spleen-derived sEVs in AMI, we used GW4869, a well-characterized pharmacological inhibitor that suppresses ceramide-mediated sEVs formation and release by targeting neutral sphingomyelinase (N-Smase). Initial safety experiments demonstrated that intraperitoneal administration of GW4869 (2.5 mg/kg/day for consecutive three days) did not induce cardiac toxicity, in terms of CK-MB levels, TNF-α and IL-10 mRNA expression, cardiac function, cardiac fibrosis, and myocardial structure, as evaluated by qPCR, echocardiography, TTC staining, H&E, and Masson's trichrome staining (Figure S7A-S7I). A single dose of GW4869 injection reduced spleen-derived sEVs protein content for one day, with levels comparable to the vehicle group thereafter (Figure S8A), suggesting its inhibitory effects on sEVs biogenesis in the spleen are short-lived. Thus, daily injections were used for subsequent studies (Figure 4A).

Under AMI conditions, GW4869 administration significantly decreased survival,

reduced left ventricular ejection fraction and fractional shortening, while increased infarct area compared with the vehicle group (Figure 4B-4G). Additionally, GW4869 treatment exacerbated adverse remodeling and injury, evidenced by elevated collagen deposition, increased protein expression of Col, FN, α-SMA, worse myocardial structural disarray, and higher serum CK-MB levels (Figure 4H-4K, Figure S8B and S8C). Pro-apoptotic markers Bax and C-Cas-3 were also upregulated, whereas anti-apoptotic Bcl2 was downregulated in ischemic hearts following GW4869 treatment (Figure 4L-M). Furthermore, GW4869 aggravated MI-induced cardiac hypertrophy (Figure 4N-O). Importantly, the deleterious effects of GW4869 were rescued by the administration of M3D-sEVs, but not by sEVs from sham mice (S-sEVs) (Figure 4A-4O, Figure S8B and S8C). These findings demonstrate that the release of spleen-derived sEVs during AMI plays an endogenously protective role against cardiac damage and adverse remodeling.

Spleen-derived sEVs improve myocardial mitochondria energy metabolism

To explore the mechanisms underlying the cardioprotective effects of M3D-sEVs, we performed 4D-proteomic profiling to compare the protein cargo of spleen-derived sEVs from sham and AMI mice (Figure 5A). A total of 1068 differentially expressed proteins (DEPs) were identified (M3D-sEVs vs S-sEVs), with 389 up-regulated and 679 down-regulated proteins in M3D-sEVs relative to S-sEVs (Figure 5B). GO enrichment analysis showed that these DEPs are associated with metabolic process, transport, intracellular organelle, electron transfer activity, and structural molecular

activity (Figure 5C-5E). KEGG pathway analysis demonstrated that they were mainly enriched in oxidative phosphorylation, metabolic pathways, and cardiac muscle contraction (Figure 5F). These results suggest that mitochondrial metabolism-related oxidative phosphorylation (OXPHOS) may serve as a key mechanism by which M3D-sEVs alleviate injury in acute myocardial infarction (AMI). We next examined mitochondrial energy metabolism, a critical determinant of myocardial response to ischemic injury. As shown in Figure 6A-6B, M3D-sEVs treatment alleviated MI-induced abnormalities in cardiac mitochondrial morphology, including restoration of organized mitochondrial cristae, preservation of myofibril integrity and recovery of mitochondrial size. These protective effects were not observed in mice treated with spleen-derived sEVs from Sham controls.

To further elucidate the impact of spleen-derived sEVs in mitochondrial function, we assessed the expression of genes and proteins associated with the mitochondrial electron transport chain (ETC) complexes in cardiac tissue. Immunoblot analysis demonstrated that protein levels of mitochondrial complex I (NDUFB8), complex II (SDHB), complex IV (MTCO1), and complex V (ATP5A) were significantly reduced in hearts from MI mice, while they were restored by M3D-sEVs treatment. In contrast, expression of complex III (UQCRC2) remained unchanged across experimental groups (Figure 6C-6F). Supporting these observations, qPCR analysis revealed significant downregulation of ETC subunit mRNA expression, including complex I (Ndufs1 and Ndufs2), complex II (Sdhc and Sdhd), complex III (Uqcrfs1 and Uqcrc1), complex IV (Cox4il) and complex V (Atp5po and Atp5f1b) in ischemic myocardial

tissue and OGD-insulted H9C2 cells, which was significantly rescued by M3D-sEVs but not S-sEVs administration (Figure 6G-6Q). These findings suggest that spleen-derived M3D-sEVs prevent ischemia-induced disruption of the cardiac mitochondrial ETC.

We next extended our investigation of energy metabolism in cardiomyocytes using H9C2 cells. M3D-sEVs but not S-sEVs treatment restored ATP/ADP ratio in OGD-insulted cells compared with those treated with vehicle (Figure 6R). In addition, M3D-sEVs treatment improved the oxygen consumption rate (OCR) in H9C2 cells subjected to OGD and attenuated abnormal mitochondrial superoxide production, as examined by mitoSOX staining (Figure 6S-6U). Collectively, these data suggest that the cardioprotective effects of M3D-sEVs in AMI are mediated, at least in part, by mitigation of mitochondrial injury and restoration of mitochondrial energy metabolism when hearts suffered from ischemic stress.

MPC1 protein expression is increased in M3D-sEVs from AMI mouse and in circulating plasma sEVs from AMI patients.

To identify critical cardioprotective factors inside M3D-sEVs, we performed proteomic profiling to compare the protein of plasma from sham and AMI mice (Figure S9). When cross-referenced with DEPs between plasma and sEVs proteomics, 21 upregulated and 12 downregulated overlapping proteins were found by using Venn diagrams (Figure 7A, Table S4). We then focused on mitochondrial energy

metabolism-related proteins, and selected MPC1 and PCK2 accordingly for further validation as their changes were most significant among these proteins. As shown in Figure 7B-7C, MPC1 protein expression was significantly increased in M3D-sEVs relative to S-sEVs, while PCK2 levels remain unchanged. Furthermore, when comparing sEVs from multiple organs post-AMI, increased MPC1 protein was uniquely observed in spleen-derived sEVs but not in sEVs from other tissues (Figure 7D). Notably, MPC1 was even decreased in sEVs from the heart and lung of AMI mice. Moreover, to assess the potential clinical relevance of MPC1 in ischemic heart disease, we determined MPC1 expression in plasma-derived sEVs from human subjects (Figure 7E). The baseline parameters of recruited patients are summarized in Table S5. TEM images and nFCM analysis confirmed the successful isolation of plasma sEVs (P-sEVs), which showed a diameter in the range of 30-200nm (Figure 7F-7G). Additionally, P-sEVs preparations were positive for marker proteins (CD63, CD9, and TSG101) and negative for GM130 and TBP (Figure 7H), confirming sample purity. As shown in Figure 7I-7J, quantification analysis exhibited that plasma sEVs-MPC1 protein levels were significantly higher in AMI patients than that in patients with CHD without MI, as well as in patients without CHD. Plasma MPC1 protein was significantly increased in AMI patients but not in CHD without AMI when compared with that in these without CHD. These clinical findings imply that sEVs-encapsulated MPC1 elevates in response to ischemic conditions in hearts.

Increased MPC1 expression accounts for the regulatory effects of M3D-sEVs

on myocardial mitochondrial energy metabolism

We neutralized MPC1 in M3D-sEVs using a specific antibody (sEVs+Ab) and administered it via intramyocardial injection in AMI mice. This neutralization significantly reduced the beneficial effects of M3D-sEVs, shown by decreased survival rates (Figure 8A), worsened cardiac function (Figure 8B-8D), increased infarct size (Figure 8E-8F), and elevated cardiac fibrosis and levels of fibrosis-related proteins (Col, FN, and α-SMA) (Figure 8G-8J). Additionally, MI-induced increase in cardiomyocyte area was more pronounced with MPC1 antagonism compared to M3D-sEVs treatment alone or M3D-sEVs incubated with control IgG (Figure 8K-8L). To further validate the role of MPC1, we employed MPC1 inhibitors, including UK5099 and GW604714x (GWx), to explore whether MPC1 contributes to the therapeutic outcomes of M3D-sEVs. As expected, both MPC1 inhibitors reduced mitochondrial pyruvate levels in H9C2 cells (Figure S10A-S10B) and were used at concentrations of 2.5 μM and 60 nM, respectively, for subsequent investigations. The inhibition of MPC1 with either compound abolished the beneficial effects of M3D-sEVs on ETC complex subunit mRNA expression in AMI hearts (Figure 8M-8Q). Specifically, both inhibitors significantly blunted the beneficial outcomes of M3D-sEVs in mitochondrial morphological characteristics as shown by TEM (Figure 8R-8S), ATP/ADP ratio, and oxygen consumption rate under OGD conditions (Figure 8T-8U). These results demonstrate that the overall cardioprotective effects of M3D-sEVs were substantially suppressed by MPC1 inhibition.

Discussion

In this study, we uncovered a novel mechanism accounting for spleen-heart crosstalk, providing compelling evidence that spleen-derived sEVs exert endogenous cardioprotective effects in AMI through enhancing delivery of MPC1. Our findings demonstrate that splenic sEVs biogenesis is dramatically upregulated following AMI, and these vesicles significantly attenuate ischemic cardiac damage in recipient mice. Moreover, MPC1 cargo is significantly increased in spleen-derived sEVs from AMI mice and is critical in the protective effects of these sEVs on ischemic myocardium. These results advance our understanding of the spleen's protective role in the early phase of AMI, highlighting a pathway whereby increasing sEVs biogenesis facilitates the delivery of MPC1 to injured myocardial tissue, and thus to improve mitochondrial energy metabolism. To our knowledge, this is the first study to identify spleen-derived sEVs as a mediator of spleen-heart crosstalk under ischemic conditions.

The concept of a cardio-splenic axis as a critical regulator of ischemic heart disease is well supported by previous studies.[3,27]. Increased metabolic activity of spleen was observed patients with acute coronary syndrome, which was measured by $^{(18)}$F-fluorodeoxyglucose-positron emission tomography imaging, and it was associated with systemic proinflammatory status and higher risks in cardiovascular disease events[28]. In rodent models, myocardial ischemia leads to splenic hypertrophy[29], and myocardial ischemia/reperfusion (I/R) results in a rapid upregulation of splenic leukocyte mobilization-related gene expression (4h post reperfusion)[30]. Consistent with these reports, we observed acute splenic activation

post AMI in mice, characterized by increased spleen size, splenic weight, and expansion of the white pulp area and marginal zone, as well as elevated expression of inflammatory cytokines (IL-6, IFN-γ, TNF-α, IL-10) in the spleen, which is consistent with Huizhen Lv and colleagues' study[31]. These findings support the notion that the spleen responds dynamically to myocardial injury, possibly through recognition of damage-associated molecular patterns derived from the ischemic heart[27]. It was reported that indigenous Bajau people who could dive to 70 meters underneath sea and were highly tolerant to diving-induced hypoxia, having increased spleen size compared to their neighbor population, the Saluan[32]. This indicates that enlarging spleen size post MI in mice might increase hypoxia tolerance to cardiac ischemia.

The role of spleen in ischemic heart disease remains controversial. Recently, Qiang Long and colleagues reported that splenectomy inhibited the infiltration of phagocytic monocytes into the injured myocardium at the early phases and eventually improved cardiac functions in I/R mice with ischemia for 60 min[30]. Similarly, splenectomy significantly reduced cardiac infarct size in mice with ischemia for 40/50 min and subsequent reperfusion for 60 min by lowering neutrophil infiltration in ischemic myocardium. Moreover, the investigation in mice also showed that AMI enhanced platelet releasing from spleen to facilitate myocardial inflammation, while splenectomy blocked platelets and leucocytes accumulation in heart, reduced infarct size, and improved cardiac functions[33]. In contrast, the epidemiological data from World War II veterans suggest that splenectomy increases mortality rates following

527 myocardial infarction[34]. In consistent with this reports, a recent study showed that
528 splenectomy suppressed inflammation and exerted beneficial outcomes in long term
529 cardiac repair in AMI mice[23]. Our data demonstrate that splenectomy immediately
530 prior to MI surgery exacerbates cardiac injury and fibrosis, while reduced the survival
531 rates in mice, supporting that spleen works as a cardioprotective function in the early
532 phase of AMI. This is further supported by studies showing that remote ischemic
533 conditioning or neuromodulation in rats and pigs enhances the release splenic
534 cardioprotective factors, where splenectomy abrogates the deploying of these splenic
535 factors and blunts the cardiac protective effects of remote ischemic condition[3,35].
536 However, the precise nature of these protective factors has remained elusive.
537 Previous studies have focused predominantly on the role of splenic immune cells in
538 modulating post ischemic injury[30]. A set of studies demonstrated that splenic
539 neutrophils, monocytes, and lymphocytes could be rapidly released into circulation
540 post ischemic insults in hearts[30,33,36]. The splenic immune cells exhibit dual roles in
541 ischemic cardiac injury. For example, Ly6C^{hi} monocytes deployed from subcapsular
542 red pulp of the spleen infiltrate to the infarct region of ischemic hearts, while inhibiting
543 Ly6C high monocyte infiltration promotes cardiac repair and improves cardiac
544 function after AMI[36]. In contrast, the injection of regulatory T cells (Tregs) enhanced
545 cardiac repair post AMI, showing as improved ejection fraction and decreased cardiac
546 fibrosis[37]. Recently, Mohamed Ameen Ismahil and colleagues found splenic
547 CD169^{+}Tim4^{+} marginal metalophulid macrophages from marginal zone of spleen
548 increased in blood 24h post AMI, and these cells alleviated inflammation and restored

cardiac function after AMI in mice[23]. The dual and context-dependent roles of these cells have complicated the development of targeted therapies for ischemic heart disease. This complexity prompted us to investigate alternative mechanisms of spleen-heart communication, focusing on sEVs as potential mediators.

sEVs have emerged as critical factors mediating intercellular and interorgan communication [38,39], modulating the pathophysiology of ischemic heart disease by delivering diverse biomolecules, including proteins, microRNAs, and lipids[40,41]. Our transcriptomic analysis revealed that genes associated with extracellular vesicle biology are upregulated in the spleen following AMI, prompting us to characterize the temporal dynamics and functional properties of spleen-derived sEVs. We found that splenic sEVs release peaks at day 3 post-AMI (M3D-sEVs), and that the administration of these vesicles to recipient AMI mice markedly attenuates cardiac injury, improves systolic function, and increases survival. These findings are consistent with emerging evidence that organ-specific sEVs can modulate inflammation, promote tissue repair, and limit ischemic injury[42]. Specifically, our results suggest that splenic sEVs may deliver reparative cargo biomolecules, such as proteins or regulatory RNAs, to the injured myocardium, coordinating beneficial immune and metabolic responses.

In this study, proteomic profiling of M3D-sEVs identified significant enrichment of proteins involved in oxidative phosphorylation, with MPC1 showing as a key candidate. Both specific antibody-mediated neutralization and pharmacological inhibition of MPC1 abolished the cardioprotective effects of M3D-sEVs, implicating

this protein as a critical effector. Importantly, increased MPC1 expression was unique to spleen-derived sEVs post AMI in mice and not observed in sEVs from other main organs. Functionally, M3D-sEVs enhanced MPC1 expression in recipient cardiomyocytes, improved mitochondrial ATP/ADP ratios, while reduced mitochondrial ROS generation, which are the hallmarks of optimized mitochondrial bioenergetics and reduced oxidative stress. These findings were further supported by our clinical data, which revealed significantly higher MPC1 levels in plasma sEVs from AMI patients compared to non-AMI CHD patients, underscoring the translational relevance of this mechanism.

MPC1 is responsible for mitochondrial pyruvate import, a critical step in maintaining intracellular pyruvate and lactate balance and limiting lactate accumulation[43,44]. Previous studies have shown that impaired pyruvate metabolism and mitochondrial dysfunction exacerbate ischemic injury and that MPC1 downregulation is associated with heart failure and increased susceptibility to cell death[16,45,46]. Besides, Yue Liu and colleges demonstrated that MPC1 downregulation enhances susceptibility to ischemic injury by increasing mitochondria disruption, oxidative stress, calcium overload, and autophagy in cortical neurons[47]. Conversely, augment MPC1 expression or activity have been shown to restore mitochondrial metabolism and ameliorate cardiomyocyte injury in models of ischemia-reperfusion. Our findings extend this paradigm by demonstrating that M3D-sEVs-mediated delivery of MPC1 constitutes a novel, endogenous rescue pathway during AMI. The observed mitochondrial benefits, such as preserved ATP generation and reduced ROS

accumulation, highlight the importance of maintaining efficient mitochondrial pyruvate flux for cardioprotection during acute ischemic stress. Thus, splenic sEVs-mediated delivery of MPC1 represents a promising therapeutic axis for preserving mitochondrial function during acute ischemia, warranting further mechanistic study and consideration for translational application in AMI.

Clinically, we observed that plasma MPC1 levels are elevated not only in AMI patients but also in those with non-AMI CHD compared to non-CHD controls, suggesting a close association between sEVs-MPC1 and the severity of coronary heart disease. Importantly, sEVs-associated biomarkers offer distinct advantages over traditional markers such as troponins. They are stable in circulation, reflect dynamic pathophysiological changes, and may provide organ-specific information[48]. Recent work indicates that most plasma sEVs were derived from spleen in AMI patients[12], supporting the feasibility of clinical investigations into splenic sEVs. The upregulation of MPC1 in plasma sEVs in patients with ischemic heart disease may reflect acute myocardial metabolic stress and mitochondrial adaptation, and sEVs-encapsulated MPC1 could serve as a potential novel circulating biomarker for early AMI diagnosis. In addition, sEVs-based platforms have demonstrated feasibility for early, minimally invasive detection of various cardiac and non-cardiac conditions[49]. Our findings suggest that plasma sEVs-MPC1, alone or in combination with established markers such as troponins and natriuretic peptides, potentially enhance the diagnostic accuracy for AMI, especially in challenging clinical scenarios or during the early phase of myocardial injury. Larger prospective studies are warranted to validate the

diagnostic performance of sEVs-MPC1 and to establish standardized quantification protocols and assess its utility in risk stratification and monitoring therapeutic response in patients with suspected acute coronary syndromes.

Despite these promising findings, several limitations should be acknowledged. First, our murine data and initial clinical data, while highly suggestive, may not fully capture the complexity of sEVs biology and MPC1 regulation in humans. The clinical cohort was modest in size and from a single center, potentially limiting generalizability. Second, although we provide convincible evidence for the role of MPC1-enriched spleen-derived sEVs in enhancing mitochondrial function and cardioprotection, the precise molecular mechanisms underlying sEVs-MPC1 delivery, cardiac uptake, and downstream signaling pathways require further elucidation. Finally, the temporal kinetics of splenic sEVs-MPC1 elevation following AMI was not fully characterized in this study.

In summary, our study reveals that spleen-derived sEVs carrying MPC1 exerting significant cardioprotective effects by enhancing mitochondrial energy metabolism and reducing oxidative stress in ischemic myocardium. We further demonstrate that plasma sEVs-MPC1 levels are elevated in AMI patients, suggesting their potential as a novel, clinically relevant biomarker for acute myocardial injury. Together, these findings uncover a previously unrecognized role for spleen–heart crosstalk mediated by splenic sEVs and highlight sEVs-MPC1 as both a mechanistic effector and a translational target in ischemic heart disease.

Acknowledgements

None.

Source of Funding

This work was supported by the National Natural Science Foundation of China (82370281 to L.Q.Z.), the Science and Technology Development Special Fund Competitive Allocation Project of Zhanjiang City (2021A05086 to W.L.C.), the High-level Talent Startup Fund (23H03, W.L.C.), Special Project for Clinical and Basic Sci&Tech Innovation of Guangdong Medical University (GDMULCJC2024048, W.L.C.), Guangdong Basic and Applied Basic Research Foundation (2025A1515010473, W.L.C.).

Disclosures

None.

Supplemental Material

Supplemental Methods

Tables S1-S5

Figure S1-S10

References 50-61

References

1. Saito Y, Oyama K, Tsujita K, Yasuda S, Kobayashi Y. Treatment strategies of acute myocardial infarction: updates on revascularization, pharmacological therapy, and beyond. *J*

661 *Cardiol*. 2023;81:168-178. doi: 10.1016/j.jjcc.2022.07.003

662 2. Rein H. [The role of the spleen and liver in coronary or hypoxic myocardial insufficiency].
663 *Pflugers Arch Gesamte Physiol Menschen Tiere*. 1951;253:435-458. doi:
664 10.1007/BF00370032

665 3. Heusch G, Kleinbongard P. The spleen in ischaemic heart disease. *Nat Rev Cardiol*. 2025. doi:
666 10.1038/s41569-024-01114-x

667 4. Tian Y, Miao B, Charles EJ, Wu D, Kron IL, French BA, Yang Z. Stimulation of the Beta2
668 Adrenergic Receptor at Reperfusion Limits Myocardial Reperfusion Injury via an
669 Interleukin-10-Dependent Anti-Inflammatory Pathway in the Spleen. *Circ J*.
670 2018;82:2829-2836. doi: 10.1253/circj.CJ-18-0061

671 5. Lieder HR, Paket U, Skyschally A, Rink AD, Baars T, Neuhauser M, Kleinbongard P, Heusch
672 G. Vago-splenic signal transduction of cardioprotection in humans. *Eur Heart J*.
673 2024;45:3164-3177. doi: 10.1093/eurheartj/ehae250

674 6. Rohm TV, Cunha ERK, Olefsky JM. Metabolic Messengers: small extracellular vesicles. *Nat*
675 *Metab*. 2025;7:253-262. doi: 10.1038/s42255-024-01214-5

676 7. Xiao J, Sluijter JPG. Extracellular vesicles in cardiovascular homeostasis and disease:
677 potential role in diagnosis and therapy. *Nat Rev Cardiol*. 2025. doi:
678 10.1038/s41569-025-01141-2

679 8. Kumar MA, Baba SK, Sadida HQ, Marzooqi SA, Jerobin J, Altemani FH, Algehainy N, Alanazi
680 MA, Abou-Samra AB, Kumar R, et al. Extracellular vesicles as tools and targets in therapy for
681 diseases. *Signal Transduct Target Ther*. 2024;9:27. doi: 10.1038/s41392-024-01735-1

682 9. Li H, Ding J, Liu W, Wang X, Feng Y, Guan H, Chen Z. Plasma exosomes from patients with

683 acute myocardial infarction alleviate myocardial injury by inhibiting ferroptosis through
684 miR-26b-5p/SLC7A11 axis. *Life Sci*. 2023;322:121649. doi: 10.1016/j.lfs.2023.121649
685 10. Duan S, Wang C, Xu X, Zhang X, Su G, Li Y, Fu S, Sun P, Tian J. Peripheral Serum
686 Exosomes Isolated from Patients with Acute Myocardial Infarction Promote Endothelial Cell
687 Angiogenesis via the miR-126-3p/TSC1/mTORC1/HIF-1alpha Pathway. *Int J Nanomedicine*.
688 2022;17:1577-1592. doi: 10.2147/IJN.S338937
689 11. Wang B, Cao C, Han D, Bai J, Guo J, Guo Q, Li D, Zhang J, Zhang Z, Wang Y, et al.
690 Dysregulation of miR-342-3p in plasma exosomes derived from convalescent AMI patients
691 and its consequences on cardiac repair. *Biomed Pharmacother*. 2021;142:112056. doi:
692 10.1016/j.biopha.2021.112056
693 12. Jin X, Xu W, Wu Q, Huang C, Song Y, Lian J. Detecting early-warning biomarkers associated
694 with heart-exosome genetic-signature for acute myocardial infarction: A source-tracking study
695 of exosome. *J Cell Mol Med*. 2024;28:e18334. doi: 10.1111/jcmm.18334
696 13. Thygesen K, Alpert JS, Jaffe AS, Chaitman BR, Bax JJ, Morrow DA, White HD, Mickley H,
697 Crea F, Van de Werf F, et al. [Fourth universal definition of myocardial infarction (2018)].
698 *Kardiol Pol*. 2018;76:1383-1415. doi: 10.5603/KP.2018.0203
699 14. Yang R, Ruan B, Wang R, Zhang X, Xing P, Li C, Zhang Y, Chang X, Song H, Zhang S, et al.
700 Cardiomyocyte betaII spectrin plays a critical role in maintaining cardiac function by regulating
701 mitochondrial respiratory function. *Cardiovasc Res*. 2024;120:1312-1326. doi:
702 10.1093/cvr/cvae116
703 15. Ong SB, Samangouei P, Kalkhoran SB, Hausenloy DJ. The mitochondrial permeability
704 transition pore and its role in myocardial ischemia reperfusion injury. *J Mol Cell Cardiol*.

705 2015;78:23-34. doi: 10.1016/j.yjmcc.2014.11.005

706 16. Visker JR, Cluntun AA, Velasco-Silva JN, Eberhardt DR, Cedeno-Rosario L, Shankar TS,
707 Hamouche R, Ling J, Kwak H, Hillas JY, et al. Enhancing mitochondrial pyruvate metabolism
708 ameliorates ischemic reperfusion injury in the heart. *JCI Insight*. 2024;9. doi:
709 10.1172/jci.insight.180906

710 17. Gray LR, Tompkins SC, Taylor EB. Regulation of pyruvate metabolism and human disease.
711 *Cell Mol Life Sci*. 2014;71:2577-2604. doi: 10.1007/s00018-013-1539-2

712 18. Fernandez-Caggiano M, Prysyazhna O, Barallobre-Barreiro J, CalvinoSantos R, Aldama
713 Lopez G, Generosa Crespo-Leiro M, Eaton P, Domenech N. Analysis of Mitochondrial
714 Proteins in the Surviving Myocardium after Ischemia Identifies Mitochondrial Pyruvate Carrier
715 Expression as Possible Mediator of Tissue Viability. *Mol Cell Proteomics*. 2016;15:246-255.
716 doi: 10.1074/mcp.M115.051862

717 19. Zhao S, Zhang Y, Bao S, Jiang L, Li Q, Kong Y, Cao J. A novel HMGA2/MPC-1/mTOR
718 signaling pathway promotes cell growth via facilitating Cr (VI)-induced glycolysis. *Chem Biol*
719 *Interact*. 2024;399:111141. doi: 10.1016/j.cbi.2024.111141

720 20. Lewis SM, Williams A, Eisenbarth SC. Structure and function of the immune system in the
721 spleen. *Sci Immunol*. 2019;4. doi: 10.1126/sciimmunol.aau6085

722 21. Mebius RE, Kraal G. Structure and function of the spleen. *Nat Rev Immunol*. 2005;5:606-616.
723 doi: 10.1038/nri1669

724 22. Zhang X, Fang Y, Qin X, Zhang Y, Kang B, Zhong L, Liu B, Luo J, Wei Y. The Role of MCPIP1
725 in Macrophage Polarization and Cardiac Function Post-Myocardial Infarction. *Adv Sci (Weinh)*.
726 2025:e2500747. doi: 10.1002/advs.202500747

727 23. Ismahil MA, Zhou G, Rajasekar S, Gao M, Bansal SS, Patel B, Limdi N, Xie M, Antipenko S,
728 Rokosh G, et al. Splenic CD169(+)Tim4(+) Marginal Metallophilic Macrophages Are Essential
729 for Wound Healing After Myocardial Infarction. *Circulation*. 2025. doi:
730 10.1161/CIRCULATIONAHA.124.071772
731 24. Rolland TJ, Hudson ER, Graser LA, Zahra S, Cucinotta D, Weil BR. Splenic Modulation of the
732 Early Inflammatory Response to Regional and Global Ischemia/Reperfusion Injury in Swine.
733 *Am J Physiol Heart Circ Physiol*. 2025. doi: 10.1152/ajpheart.00714.2024
734 25. Yu J, Sane S, Kim JE, Yun S, Kim HJ, Jo KB, Wright JP, Khoshdoozmasouleh N, Lee K, Oh
735 HT, et al. Biogenesis and delivery of extracellular vesicles: harnessing the power of EVs for
736 diagnostics and therapeutics. *Front Mol Biosci*. 2023;10:1330400. doi:
737 10.3389/fmolb.2023.1330400
738 26. Luo Y, Liu K, Ling D, Gu T, Zhang L, Chen W. Isolation and Characterization of Exosomes
739 Derived from Mouse Spleen Tissues. *J Vis Exp*. 2024. doi: 10.3791/67234
740 27. Tian Y, Pan D, Chordia MD, French BA, Kron IL, Yang Z. The spleen contributes importantly to
741 myocardial infarct exacerbation during post-ischemic reperfusion in mice via signaling
742 between cardiac HMGB1 and splenic RAGE. *Basic Res Cardiol*. 2016;111:62. doi:
743 10.1007/s00395-016-0583-0
744 28. Emami H, Singh P, MacNabb M, Vucic E, Lavender Z, Rudd JH, Fayad ZA, Lehrer-Graiwer J,
745 Korsgren M, Figueroa AL, et al. Splenic metabolic activity predicts risk of future cardiovascular
746 events: demonstration of a cardiosplenic axis in humans. *JACC Cardiovasc Imaging*.
747 2015;8:121-130. doi: 10.1016/j.jcmg.2014.10.009
748 29. Ruggiero SA, Huber JS, Murrant CL, Brunt KR, Simpson JA. Splenic blood-flow response

749 following myocardial infarction in rat. *Can J Physiol Pharmacol*. 2018;96:1060-1068. doi:
750 10.1139/cjpp-2018-0134
751 30. Long Q, Rabi K, Cai Y, Li L, Huang S, Qian B, Zhong Y, Qi Z, Zhang Y, Huang K, et al.
752 Identification of splenic IRF7 as a nanotherapy target for tele-conditioning myocardial
753 reperfusion injury. *Nat Commun*. 2025;16:1909. doi: 10.1038/s41467-025-57048-6
754 31. Lv H, Wang C, Liu Z, Quan M, Li K, Gou F, Shi X, Liu Q, Yu Y, Zhu P, et al. Suppression of the
755 Prostaglandin I2-Type 1 Interferon Axis Induces Extramedullary Hematopoiesis to Promote
756 Cardiac Repair After Myocardial Infarction. *Circulation*. 2025. doi:
757 10.1161/CIRCULATIONAHA.124.069420
758 32. Ilardo MA, Moltke I, Korneliussen TS, Cheng J, Stern AJ, Racimo F, de Barros Damgaard P,
759 Sikora M, Seguin-Orlando A, Rasmussen S, et al. Physiological and Genetic Adaptations to
760 Diving in Sea Nomads. *Cell*. 2018;173:569-580 e515. doi: 10.1016/j.cell.2018.03.054
761 33. Gao XM, Moore XL, Liu Y, Wang XY, Han LP, Su Y, Tsai A, Xu Q, Zhang M, Lambert GW, et
762 al. Splenic release of platelets contributes to increased circulating platelet size and
763 inflammation after myocardial infarction. *Clin Sci (Lond)*. 2016;130:1089-1104. doi:
764 10.1042/CS20160234
765 34. Robinette CD, Fraumeni JF, Jr. Splenectomy and subsequent mortality in veterans of the
766 1939-45 war. *Lancet*. 1977;2:127-129. doi: 10.1016/s0140-6736(77)90132-5
767 35. Lieder HR, Kleinbongard P, Skyschally A, Hagelschuer H, Chilian WM, Heusch G.
768 Vago-Splenic Axis in Signal Transduction of Remote Ischemic Preconditioning in Pigs and
769 Rats. *Circ Res*. 2018;123:1152-1163. doi: 10.1161/CIRCRESAHA.118.313859
770 36. Zhang J, Hao W, Zhang J, Li T, Ma Y, Wang Y, Li X, Cui W, Du J. CXCL16 Promotes

771 Ly6Chigh Monocyte Infiltration and Impairs Heart Function after Acute Myocardial Infarction. *J*
772 *Immunol*. 2023;210:820-831. doi: 10.4049/jimmunol.2200249
773 37. Alshoubaki YK, Nayer B, Lu YZ, Salimova E, Lau SN, Tan JL, Amann-Zalcenstein D, Hickey
774 PF, Del Monte-Nieto G, Vasanthakumar A, et al. Tregs delivered post-myocardial infarction
775 adopt an injury-specific phenotype promoting cardiac repair via macrophages in mice. *Nat*
776 *Commun*. 2024;15:6480. doi: 10.1038/s41467-024-50806-y
777 38. Huang-Doran I, Zhang CY, Vidal-Puig A. Extracellular Vesicles: Novel Mediators of Cell
778 Communication In Metabolic Disease. *Trends Endocrinol Metab*. 2017;28:3-18. doi:
779 10.1016/j.tem.2016.10.003
780 39. Hu S, Hu Y, Yan W. Extracellular vesicle-mediated interorgan communication in metabolic
781 diseases. *Trends Endocrinol Metab*. 2023;34:571-582. doi: 10.1016/j.tem.2023.06.002
782 40. Tian C, Gao L, Rudebush TL, Yu L, Zucker IH. Extracellular Vesicles Regulate
783 Sympatho-Excitation by Nrf2 in Heart Failure. *Circ Res*. 2022;131:687-700. doi:
784 10.1161/CIRCRESAHA.122.320916
785 41. Fu S, Zhang Y, Li Y, Luo L, Zhao Y, Yao Y. Extracellular vesicles in cardiovascular diseases.
786 *Cell Death Discov*. 2020;6:68. doi: 10.1038/s41420-020-00305-y
787 42. Zheng X, Hermann DM, Bahr M, Doeppner TR. The role of small extracellular vesicles in
788 cerebral and myocardial ischemia-Molecular signals, treatment targets, and future clinical
789 translation. *Stem Cells*. 2021;39:403-413. doi: 10.1002/stem.3329
790 43. Sichrovsky M, Lacabanne D, Ruprecht JJ, Rana JJ, Stanik K, Dionysopoulou M, Sowton AP,
791 King MS, Jones SA, Cooper L, et al. Molecular basis of pyruvate transport and inhibition of the
792 human mitochondrial pyruvate carrier. *Sci Adv*. 2025;11:eadw1489. doi:

793 10.1126/sciadv.adw1489

794 44. He Z, Zhang J, Xu Y, Fine EJ, Suomivuori CM, Dror RO, Feng L. Structure of mitochondrial
795 pyruvate carrier and its inhibition mechanism. *Nature*. 2025;641:250-257. doi:
796 10.1038/s41586-025-08667-y

797 45. Lesnefsky EJ, Chen Q, Tandler B, Hoppel CL. Mitochondrial Dysfunction and Myocardial
798 Ischemia-Reperfusion: Implications for Novel Therapies. *Annu Rev Pharmacol Toxicol*.
799 2017;57:535-565. doi: 10.1146/annurev-pharmtox-010715-103335

800 46. Lopez-Vazquez P, Fernandez-Caggiano M, Barge-Caballero E, Barge-Caballero G,
801 Couto-Mallon D, Grille-Cancela Z, Blanco-Canosa P, Paniagua-Martin MJ, Enriquez-Vazquez
802 D, Vazquez-Rodriguez JM, et al. Reduced mitochondrial pyruvate carrier expression in hearts
803 with heart failure and reduced ejection fraction patients: ischemic vs. non-ischemic origin.
804 *Front Cardiovasc Med*. 2024;11:1349417. doi: 10.3389/fcvm.2024.1349417

805 47. Liu Y, Yuan Y, Yan Y, Wang R, Wang Z, Liu X, Zhang Y, Hua J, Wang Y, Zhao L.
806 Mitochondrial pyruvate carrier 1 alleviates hypoxic-ischemic brain injury in rats. *Life Sci*.
807 2023;325:121686. doi: 10.1016/j.lfs.2023.121686

808 48. Garcia-Martin R, Brandao BB, Thomou T, Altindis E, Kahn CR. Tissue differences in the
809 exosomal/small extracellular vesicle proteome and their potential as indicators of altered
810 tissue metabolism. *Cell Rep*. 2022;38:110277. doi: 10.1016/j.celrep.2021.110277

811 49. Das D, Jothimani G, Banerjee A, Dey A, Duttaroy AK, Pathak S. A brief review on recent
812 advances in diagnostic and therapeutic applications of extracellular vesicles in cardiovascular
813 disease. *Int J Biochem Cell Biol*. 2024;173:106616. doi: 10.1016/j.biocel.2024.106616

814 50. Li S, Shen S, Xu H, Cai S, Yuan X, Wang C, Zhang X, Chen S, Chen J, Shi DL, et al. IGF2BP3

815 promotes adult myocardial regeneration by stabilizing MMP3 mRNA through interaction with
816 m6A modification. *Cell Death Discov*. 2023;9:164. doi: 10.1038/s41420-023-01457-3
817 51. Tian Y, French BA, Kron IL, Yang Z. Splenic leukocytes mediate the hyperglycemic
818 exacerbation of myocardial infarct size in mice. *Basic Res Cardiol*. 2015;110:39. doi:
819 10.1007/s00395-015-0496-3
820 52. Ge X, Meng Q, Wei L, Liu J, Li M, Liang X, Lin F, Zhang Y, Li Y, Liu Z, et al. Myocardial
821 ischemia-reperfusion induced cardiac extracellular vesicles harbour proinflammatory features
822 and aggravate heart injury. *J Extracell Vesicles*. 2021;10:e12072. doi: 10.1002/jev2.12072
823 53. Ge X, Meng Q, Zhuang R, Yuan D, Liu J, Lin F, Fan H, Zhou X. Circular RNA expression
824 alterations in extracellular vesicles isolated from murine heart post ischemia/reperfusion injury.
825 *Int J Cardiol*. 2019;296:136-140. doi: 10.1016/j.ijcard.2019.08.024
826 54. Zuo R, Ye LF, Huang Y, Song ZQ, Wang L, Zhi H, Zhang MY, Li JY, Zhu L, Xiao WJ, et al.
827 Hepatic small extracellular vesicles promote microvascular endothelial hyperpermeability
828 during NAFLD via novel-miRNA-7. *J Nanobiotechnology*. 2021;19:396. doi:
829 10.1186/s12951-021-01137-3
830 55. Lasser C, Kishino Y, Park KS, Shelke GV, Karimi N, Suzuki S, Hovhannisyan L, Radinger M,
831 Lotvall J. Immune-Associated Proteins Are Enriched in Lung Tissue-Derived Extracellular
832 Vesicles during Allergen-Induced Eosinophilic Airway Inflammation. *Int J Mol Sci*. 2021;22. doi:
833 10.3390/ijms22094718
834 56. Crescitelli R, Lasser C, Lotvall J. Isolation and characterization of extracellular vesicle
835 subpopulations from tissues. *Nat Protoc*. 2021;16:1548-1580. doi:
836 10.1038/s41596-020-00466-1

837 57. Jingushi K, Uemura M, Ohnishi N, Nakata W, Fujita K, Naito T, Fujii R, Saichi N, Nonomura N,
838 Tsujikawa K, et al. Extracellular vesicles isolated from human renal cell carcinoma tissues
839 disrupt vascular endothelial cell morphology via azurocidin. *Int J Cancer*. 2018;142:607-617.
840 doi: 10.1002/ijc.31080
841 58. Chen L, Li S, Zhu J, You A, Huang X, Yi X, Xue M. Mangiferin prevents myocardial
842 infarction-induced apoptosis and heart failure in mice by activating the Sirt1/FoxO3a pathway.
843 *J Cell Mol Med*. 2021;25:2944-2955. doi: 10.1111/jcmm.16329
844 59. Zielonka J, Kalyanaraman B. Hydroethidine- and MitoSOX-derived red fluorescence is not a
845 reliable indicator of intracellular superoxide formation: another inconvenient truth. *Free Radic*
846 *Biol Med*. 2010;48:983-1001. doi: 10.1016/j.freeradbiomed.2010.01.028
847 60. Mol EA, Lei Z, Roefs MT, Bakker MH, Goumans MJ, Doevendans PA, Dankers PYW, Vader P,
848 Sluijter JPG. Injectable Supramolecular Ureidopyrimidinone Hydrogels Provide Sustained
849 Release of Extracellular Vesicle Therapeutics. *Adv Healthc Mater*. 2019;8:e1900847. doi:
850 10.1002/adhm.201900847
851 61. Wisniewski JR, Zougman A, Nagaraj N, Mann M. Universal sample preparation method for
852 proteome analysis. *Nat Methods*. 2009;6:359-362. doi: 10.1038/nmeth.1322
853

Figures and Figure Legends

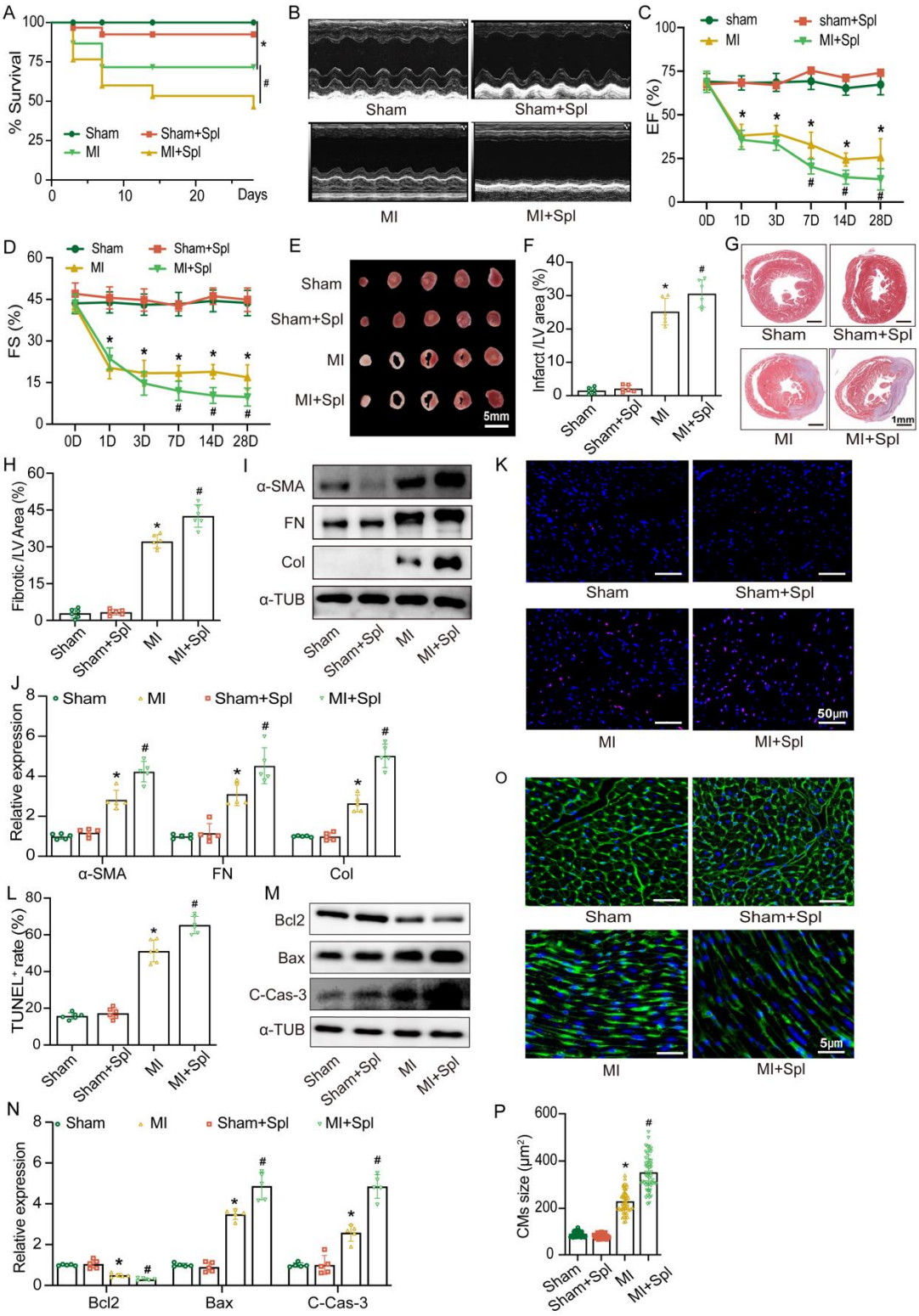

Figure 1. Splenectomy aggravates cardiac injury in AMI mice

A, Twenty-eight-day Kaplan-Meier survival curves for sham operation (Sham) or MI

mice, with or without splenectomy (n=30 mice/group). **B**, Representative echocardiograms from sham, splenectomized sham (Sham+Spl), MI, and splenectomized MI (MI+Spl) mice 7 days post MI (n=6/group). **C** and **D**, Summary of left ventricle EF (LVEF%) and FS (LVFS%) in sham, Sham+Spl, MI, and MI+Spl mice at indicated time-points (n=6/group). **E** and **F**, Representative TTC images of cross-sectional cardiac slices and Quantitation of infarct size in hearts from sham, Sham+Spl, MI, and MI+Spl mice 1 day post MI (n=6 mice per group). **G** and **H,** Representative images of Masson's trichrome staining and quantitation of the fibrosis area in hearts from sham, Sham+Spl, MI, and MI+Spl mice 14 days after MI (n=6/group). **I**-**J**, Representative western blots quantitation of collagen I, Fibronectin, and α-SMA expression in mice hearts 14 days post MI (n=6/group). **K**-**L,** Representative TUNEL images and quantitation of TUNEL-positive rates in myocardial tissues from sham, Sham+Spl, MI, and MI+Spl mice 3 days post MI (n=6/group). **M**-**N,** Representative western blots and quantitation of C-Cas-3, Bax, and Bcl2 in mice hearts 3 days post MI (n=6/group). **O**-**P**, Representative WGA staining images of cardiac sections and quantitation of cardiomyocyte size in mice hearts 28 days post MI (n=6/group). *, vs Sham; $^{\#}$, vs MI, $P<0.05$. Statistical analyses were performed using mixed-effects ANOVA followed by the Sidak multiple comparisons test (**C** and **D**), the one-way ANOVA with the Dunnett multiple comparisons test (**H**, **P** and **L**), the Brown-Forsythe and Welch ANOVA test with the Dunnett T3 multiple comparisons test (**F**, **J**; Collagen I and N; Bcl2, C-Cas-3), the one-way ANOVA with the Tukey multiple comparisons test (**J**; α-SMA and N; Bax), the

Kruskal Wallis with the Dunn multiple comparisons test (**J**; Fibronectin). Survival curve rate was analyzed by the Kaplan-Meier method and compared by the log-rank test in **A**. Spl indicates splenectomy; EF, ejection fraction; FS, fractional shortening; LV, left ventricular; FN, Fibronectin; Col, Collagen I (COL1A1); and α-TUB, α-Tubulin.

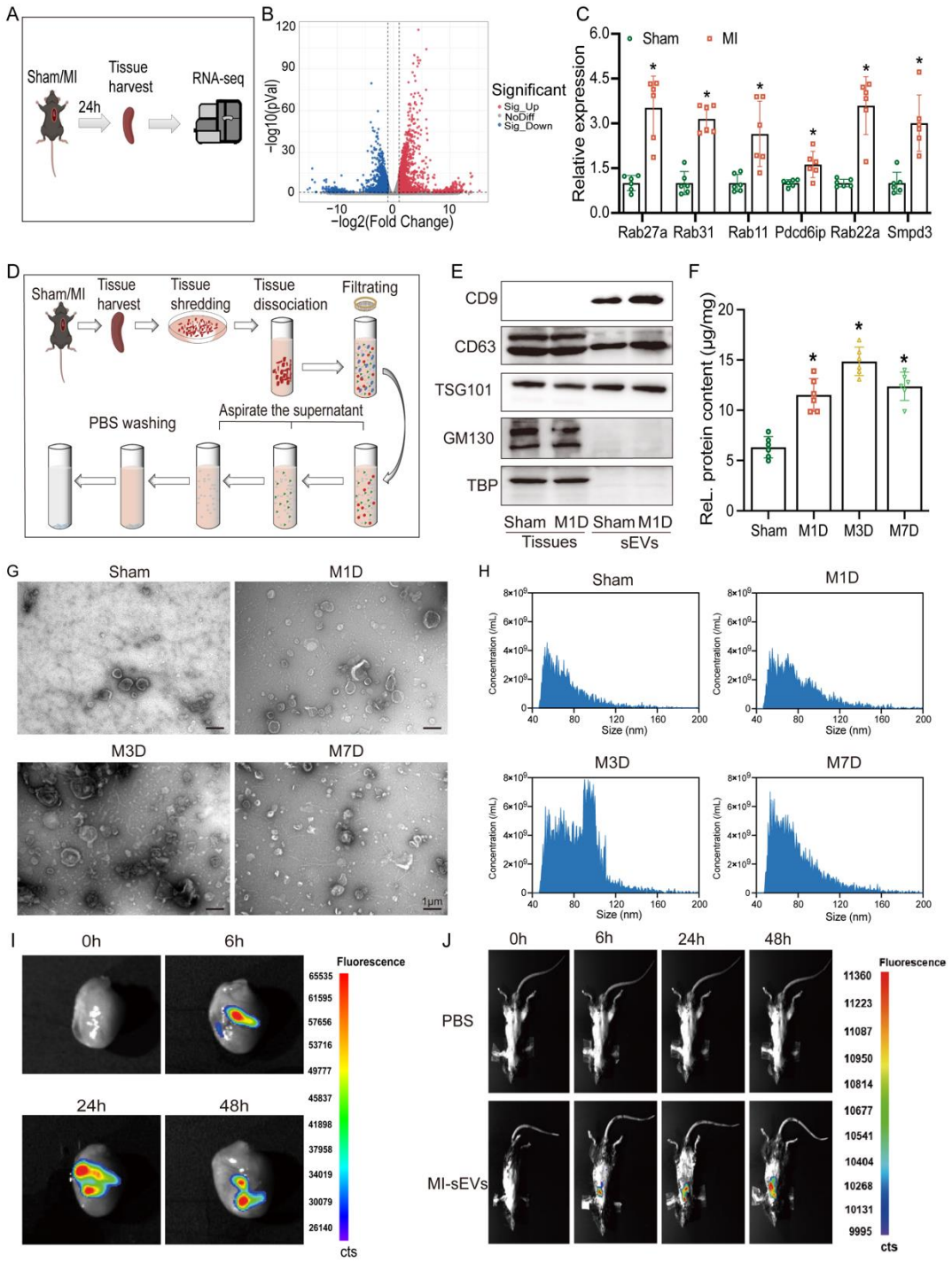

Figure 2. Spleen-derived sEVs biogenesis is enhanced in response to AMI and these sEVs were enriched in ischemic hearts in mice.

A, Schematic diagram of RNA-Seq for spleens from Sham and MI mice. **B**, Volcano plot of differentially expressed genes (DEGs) of spleens from sham and MI mice. **C**, sEVs biogenesis-related DEGs expression in spleen tissues from sham and MI mice were validated using qPCR 1 day post MI. Data were normalized to GAPDH and expressed as folds of Sham group (n=6/group). **D,** The flowchart of spleen-derived sEVs extraction. **E**, Representative western blot images of sEVs markers. **F**, Protein contents of sEVs (n=6/group). **G**, Representative TEM images of spleen-derived sEVs from various mice groups as indicated. **H**, Size distributions of Spleen-derived sEVs measured by nFCM. **I-J**, Detection of the biodistribution of DIR-labeled spleen-derived sEVs in vivo. Representative heart and whole-body images and were shown. *, vs Sham, $P<0.05$. Statistical analyses were performed by unpaired t test (**C**; Rab27a, Rab11, Pdcd6ip and Smpd3), the Mann-Whitney U test (**C**; Rab31 and Rab22a) and the one-way ANOVA with the Dunnett multiple comparisons test (**F**). M1D indicates day 1 after MI; M3D, day 3 after MI; M7D, day 7 after MI.

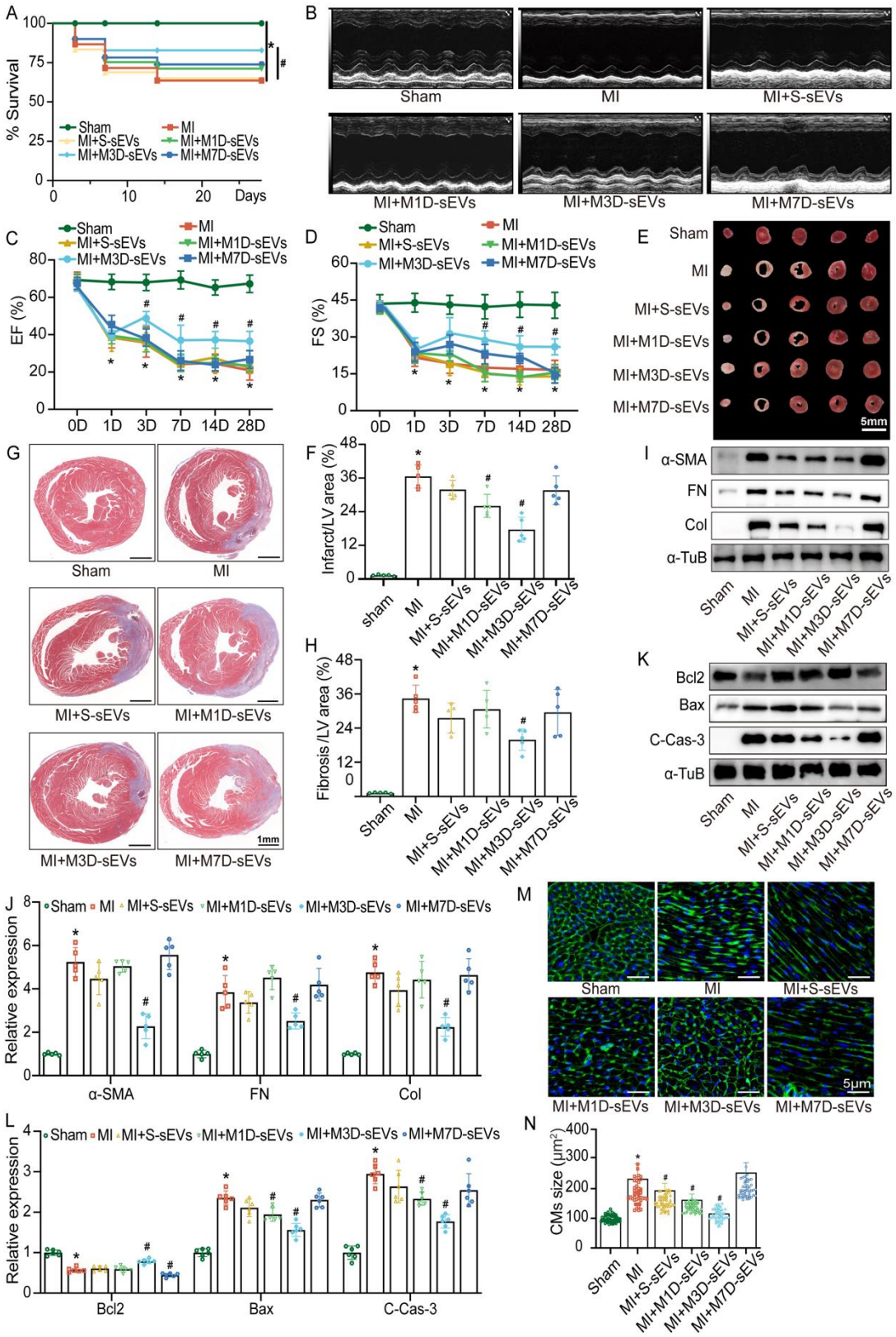

Figure 3. Spleen-derived sEVs from MI mice alleviate ischemia injuries in hearts and cardiomyocytes.

A, Twenty-eight-day Kaplan-Meier survival curves for sham or MI mice treated with indicated sEVs or vehicle (n=30 mice per group). **B-D**, Representative echocardiograms of sham or MI mice treated with indicated sEVs or vehicle 7 days after MI (n=6/group). C-D. Quantitation of LVEF% and LVFS%. **E-F**, Representative images of TTC staining and quantitation of infarct area in mice hearts 1 day after MI (n=6/group). **G-H**, Representative images of Masson's trichrome and quantitation of the scar area in mice hearts 14 days after MI (n=6/group). **I-J**, Representative western blot images and quantitation of cardiac collagen I, Fibronectin, and α-SMA 14 days after MI (n=6 mice per group). **K-L**, Representative western blot images and quantitation of cardiac C-Cas-3, Bax, and Bcl2 3 days after MI (n=6/group). **M-N**, Representative WGA staining images of cardiac sections and quantitation of cardiomyocytes (CMs) 28 days after MI (n=6/group). *, vs Sham; #, vs MI, $P<0.05$. Statistical analyses were performed using mixed-effects ANOVA followed by the Sidak multiple comparisons test (**C** and **D**), the one-way ANOVA with the Dunnett multiple comparisons test (**F** and **H**), the one-way ANOVA with the Tukey multiple comparisons test (**K**; α-SMA, Fibronectin and **L**; Bcl2, C-Cas-3), the Kruskal-Wallis with the Dunn multiple comparisons test (**K**; Collagen I and **L**; Bax), and the Brown-Forsythe and Welch-ANOVA test with the Dunnett T3 multiple comparisons test (**N**). Survival curve rate was analyzed by the Kaplan-Meier method and compared by the log-rank test in **A**. S-sEVs indicates small extracellular vesicles derived from spleens of sham mice; M1D-sEVs, sEVs derived from spleens of MI mice 1 day post MI; M3D-sEVs, sEVs derived from spleens of MI mice 3 day post MI;

and M7D-sEVs, sEVs derived from spleens of MI mice 7 day post MI. EF, ejection fraction; FS, fractional shortening; LV, left ventricular; FN, Fibronectin; Col, Collagen I (COL1A1); and α-TUB, α-Tubulin.

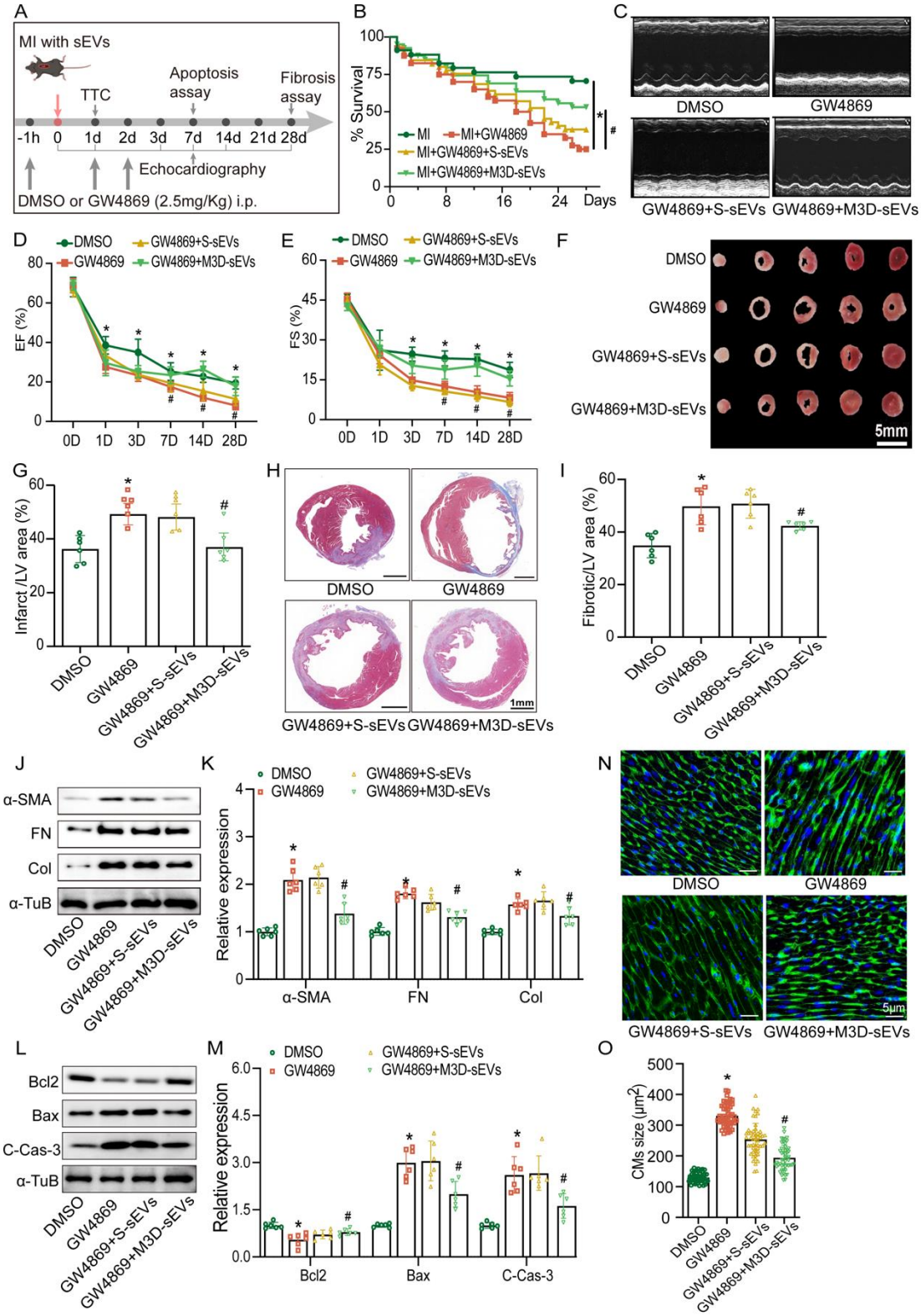

Figure 4. sEVs depletion aggravates cardiac ischemic injury in AMI mice.

A, Schematic diagram of experimental design for sEVs depletion. **B**, Twenty-eight-day Kaplan-Meier survival curves for MI mice treated with indicated conditions (n=30 mice per group). Log-rank test. **C**, Representative echocardiograms of AMI mice treated with GW4869 plus S-sEVs or M3D-sEVs, or corresponding vehicles 7 days after MI (n=6 mice per group). **D-E**, Quantitation of LVEF% and LVFS%. **F-G**, Representative images of TTC staining of cardiac slices from AMI mice treated with GW4869 plus S-sEVs or M3D-sEVs, or corresponding vehicles, and quantitation of infarct area in mice hearts 1 day after MI (n=6/group). **J-K**, Representative western blot images and quantitation of cardiac collagen I, Fibronectin, and α-SMA 14 days after MI in mice treated as indicated conditions (n=6/group). **L-M**, Representative western blot images and quantitation of cardiac C-Cas-3, Bax, and Bcl2 of hearts 3 days after MI in mice (n=6/group). **N-P**, Representative WGA staining images of cardiac sections and quantitation of cardiomyocytes (CMs) 28 days after MI (n=6/group). *, vs MI; #, vs MI+GW4869, $P<0.05$. Statistical analyses were performed using mixed-effects ANOVA followed by the Sidak multiple comparisons test (**D** and **E**), the one-way ANOVA with the Dunnett multiple comparisons test (**G**), the Brown-Forsythe and Welch-ANOVA test with the Dunnett T3 multiple comparisons test (**I** and **M**; Bax), the Kruskal-Wallis with the Dunn multiple comparisons test (**M**; C-Cas-3 and **P**), and the one-way ANOVA with the Tukey multiple comparisons test (**K** and **M**; Bcl2). Survival curve rate was analyzed by the Kaplan-Meier method and compared by the log-rank test in B. EF,

ejection fraction; FS, fractional shortening; LV, left ventricular; FN, Fibronectin; Col, Collagen I (COL1A1); and α-TUB, α-Tubulin.

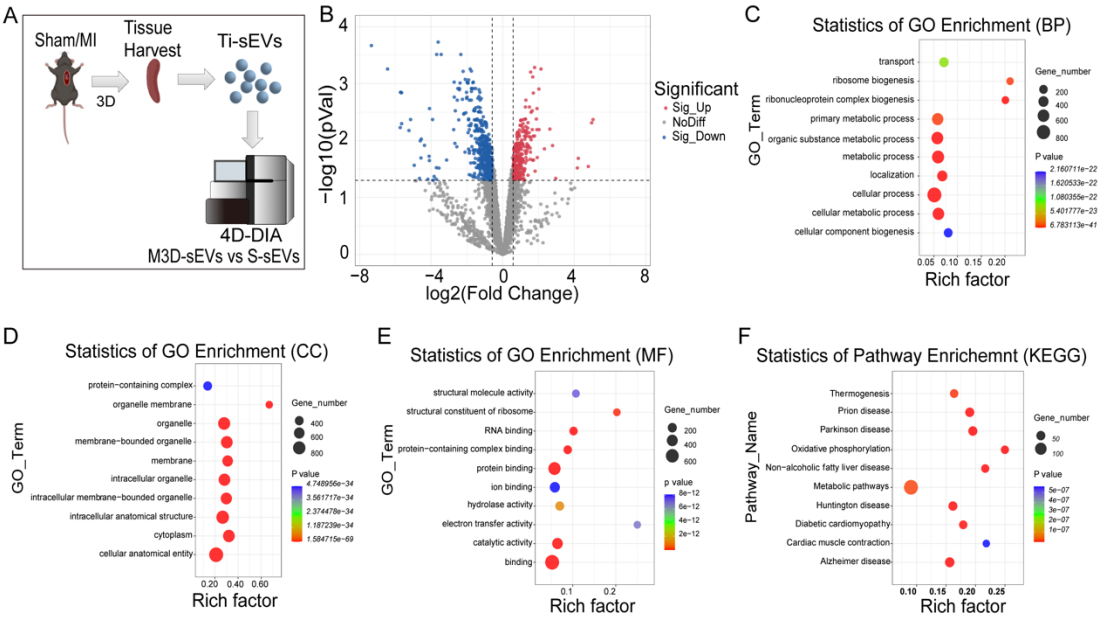

Figure 5. The proteomic profiling of spleen-derived sEVs between sham and AMI mice 3 days post ischemia.

A, The flowchart of proteomics experiment for spleens from sham and AMI mouse. **B**, Volcano plot showing the differentially expressed proteins in spleens between sham and AMI mouse. **C-E**, GO enrichment analysis of differentially expressed proteins. **F**, KEGG enrichment analysis of differentially expressed proteins. BP, Biological Process. CC, Cellular Component. MF, Molecular Function.

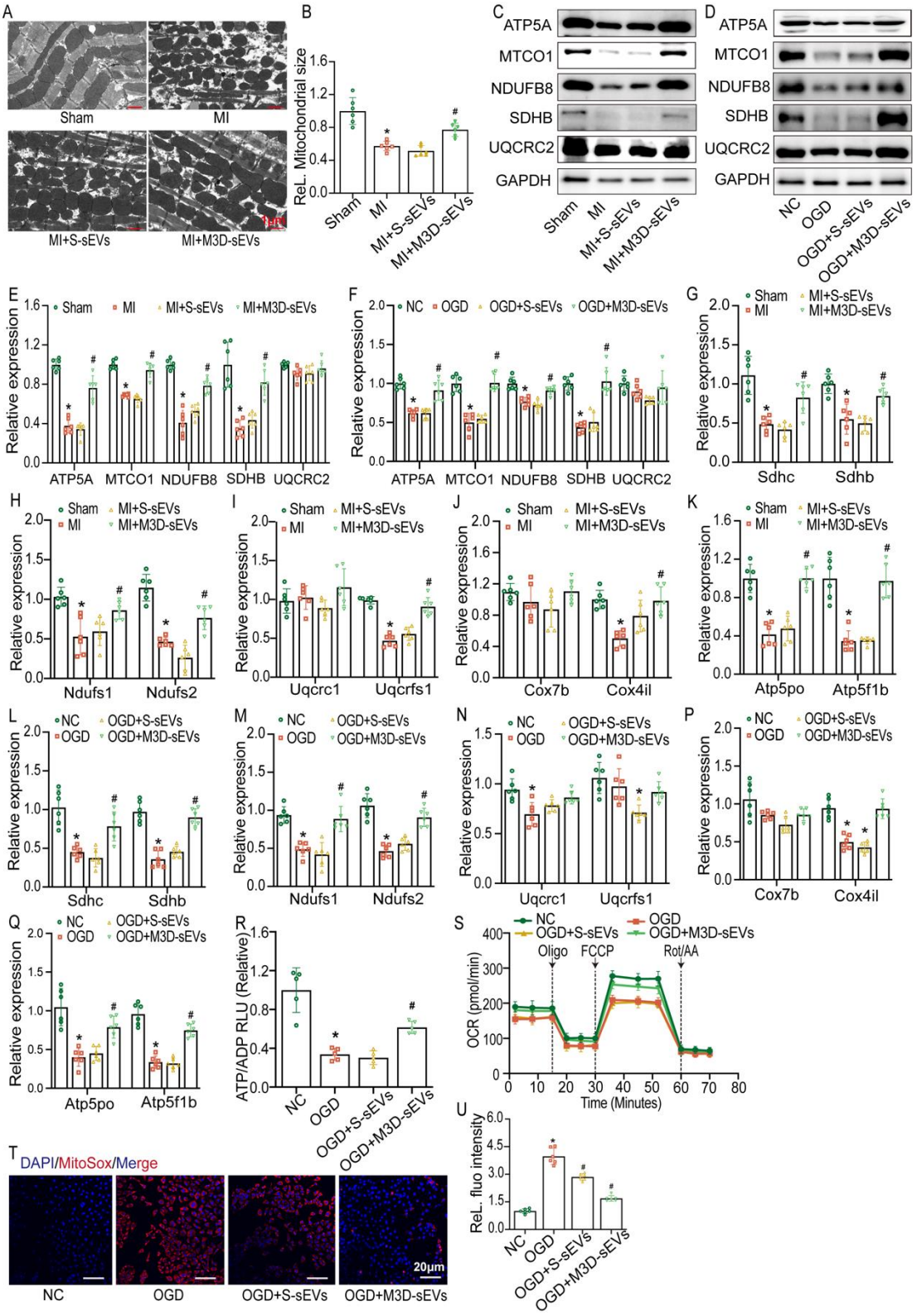

Figure 6. Spleen-derived sEVs from MI mice improve myocardial mitochondrial energy metabolism.

A, Representative TEM images showing mitochondrial ultrastructure of heart tissues from sham and MI mice treated with S-sEVs, M3D-sEVs, or vehicles. **B**, Quantitation of mitochondrial size in these TEM images as indicated groups, being presented as relative value to the sham group (n=6/group). **C-F**, Representative western blotting images and quantitation of ETC complex subunits expression in heart tissues from sham and MI mice treated with S-sEVs, M3D-sEVs, or vehicles for 7 days, and in normal control cells (NC) and OGD-insulted H9C2 cells treated with S-sEVs, M3D-sEVs, or vehicles for 12h (n=6/group). **G-K**, mRNA expressions of ETC-coded genes in the heart tissues from mice treated with as above indicated conditions (n=6/group). **L-Q**, mRNA expressions of ETC-coded genes in H9C2 cells treated as above indicated conditions (n=6/group). **R**, ATP/ADP ratios of NC and OGD-insulted H9C2 cells treated S-sEVs, M3D-sEVs, or vehicles for 24h (n=6/group). **S**, Real-time monitoring OCR in H9C2 cells treated NC and OGD-insulted H9C2 cells treated S-sEVs, M3D-sEVs, or vehicles for 12h (n=6/group). **T-U**, Representative MitoSOX staining images and quantitation of the MitoSOX fluorescent intensity in NC and OGD-insulted H9C2 cells treated S-sEVs, M3D-sEVs, or vehicles for 12h(n=6/group). *, vs Sham or NC, $P<0.05$; $^{\#}$, vs MI or OGD, $P<0.05$. Statistical analyses were performed by the one-way ANOVA with the Dunnett multiple comparisons test (**B** and **R**), the one-way ANOVA with the Tukey multiple comparisons test (**E**; ATP5A, MTCO1, NDUFB8, UQCRC2, **F**;NDUFB8, **G**; Sdhb, **H**, **I**; Uqcrc1, **J**, **K**; Atp5po, **L**; Sdhb, **M**; Ndufs2, **N** and **P**; Cox4il), the Brown-Forsythe and Welch-ANOVA test with the Dunnett T3 multiple comparisons test (**E**; SDHB, **L**; Sdhc, **P**; Cox7b, **Q** and **U**),

and the Kruskal-Wallis with the Dunn multiple comparisons test (**F**; ATP5A, MTCO1, SDHB, UQCRC2, **G**; Sdhb, **I**; Uqcrc1, **K**; Atp5f1b and **M**; Ndufs1).

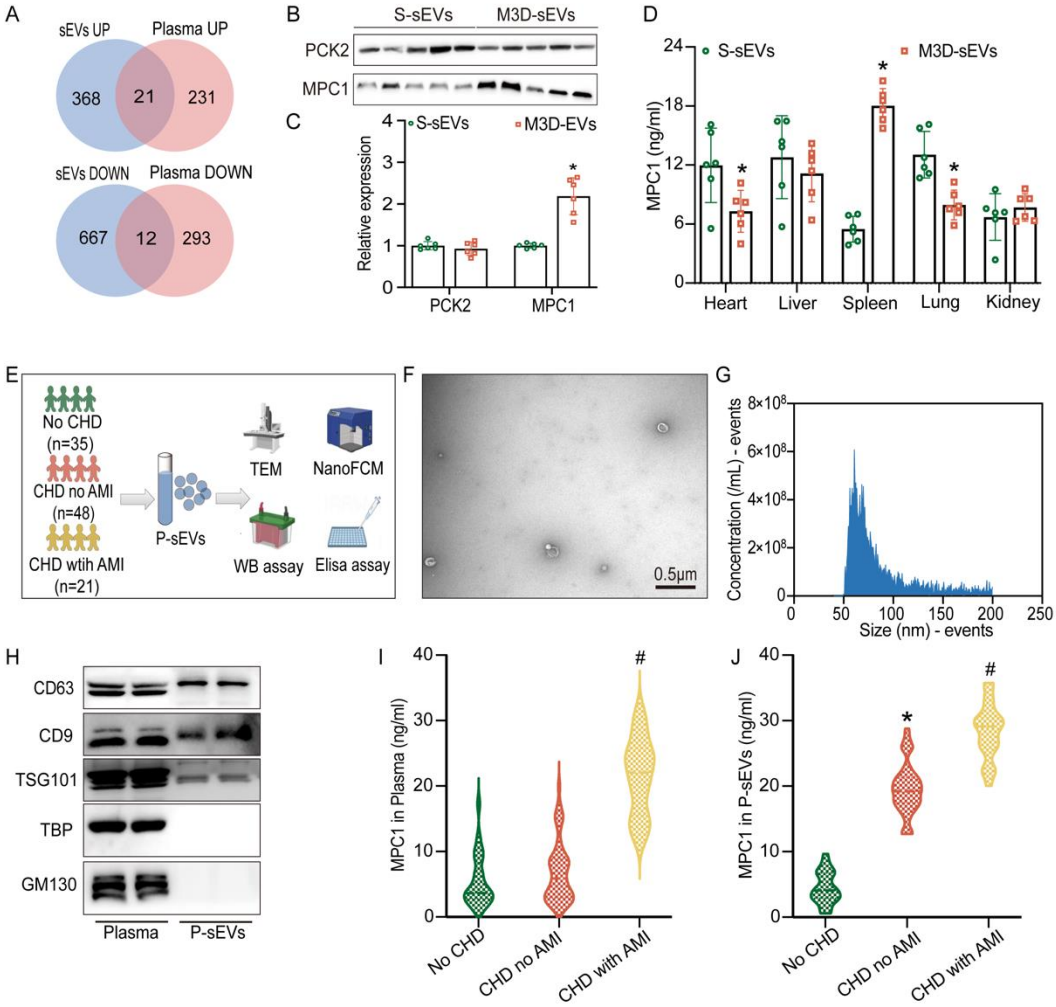

Figure 7. MPC1 protein expression is increased in M3D-sEVs from AMI mouse and in circulating plasma sEVs from AMI patients.

A, Veen diagrams of differentially expressed proteins in spleen-derived sEVs and plasma between sham and AMI mouse. **B-C**, Representative western blotting images and quantitation of MPC1 and PCK2 expression inside sEVs from sham and AMI mouse. Unpaired two-tailed Welch t-test. **D**, Quantitation results of ELISA analysis

determining MPC1 expression in organ tissues-derived sEVs after MI. unpaired t test. **E**, Schematic diagram of plasma sEVs (P-sEVs) isolation from patients. **F**, Representative TEM images of P-sEVs. **G**, Size distributions of P-sEVs measured by nFCM. **H**, Immunoblot determination of sEVs markers. **I**, ELISA assay results of the plasma MPC1 expression from patients. **J**, ELISA assay results of MPC1 expression in P-sEVs. *, vs S-sEVs or No CHD, $P<0.05$. #, vs CHD no AMI, $P<0.05$. Statistical analyses were performed by the unpaired two-tailed Welch t-test (**C**; MPC1), the unpaired t test (**C**; PCK2 and **D**), the Kruskal-Wallis with the Dunn multiple comparisons test (**I**) and the one-way ANOVA with the Dunnett multiple comparisons test (**J**). Ti-sEVs indicates tissue sEVs.

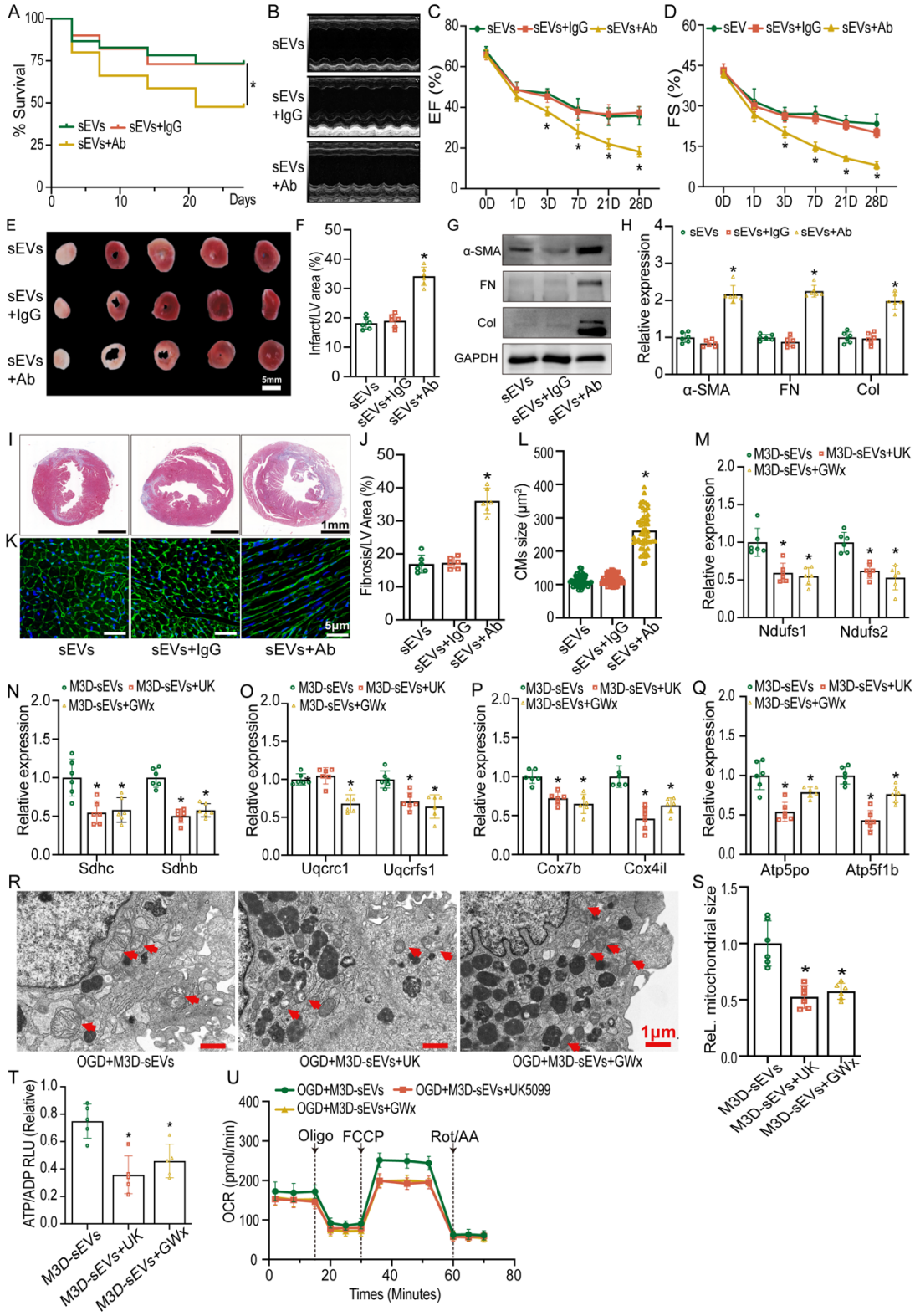

Figure 8. Blockage of MPC1 blunts the protective effects of spleen-derived M3D-sEVs against ischemic cardiac damage and disruption of myocardial mitochondrial energy metabolism.

A, Twenty-eight-day Kaplan-Meier survival curves for AMI mouse treated with M3D-sEVs (sEVs), MPC1 antibody-neutralized M3D-sEVs (sEVs+Ab), or Ig G-incubated M3D-sEVs (sEVs+IgG), n=30/group. Log-rank test. **B**, Representative echocardiograms of AMI mice treated with indicated conditions 7 days after MI (n=6/group). **C-D**, Quantitation of LVEF% and LVFS%. **E-F**, Representative TTC staining images of cross-sectional cardiac slices from AMI mice treated as above indicated 1 day post MI, and quantitation of infarct area percentage (n=6/group). **G-H**, Representative western blotting images and quantitation of cardiac collagen I, Fibronectin, and α-SMA expression in AMI mice treated as above indicated 14 days after MI (n=6/group). **I-K**, Representative images of Masson's trichrome (top) and WGA staining (bottom) and quantitation of the hearts from AMI mice treated as above indicated 14- or 28-days post MI, respectively (n=6 mice per group). **L-P**, mRNA expression of ETC-coded genes in the OGD-insulted H9C2 cells treated with M3D-sEVs or M3D-sEVs plus MPC1 inhibitors (n=6/group). **Q**, Representative TEM images showing mitochondrial ultrastructure of heart tissues from AMI mice treated as above indicated. **R**, Quantitation of mitochondrial size in TEM images as indicated groups, being presented as relative value to the M3D-sEVs group (n=6/group). **S**, Quantitation of ATP/ADP ratio of OGD-H9C2 cells treated as indicated (n=6/group). **T**, Results of OCR assay in H9C2 cells treated as indicated. Statistical analyses were performed using mixed-effects ANOVA followed by the Sidak multiple comparisons test (**C** and **D**), the one-way ANOVA with the Dunnett multiple comparisons test (**F**, **J** and **S**), the one-way ANOVA with the Tukey multiple comparisons test (**H**; Collagen I,

L; Ndufs2, **M**, **N**, **O** and **P**), the Brown-Forsythe and Welch-ANOVA test with the Dunnett T3 multiple comparisons test (**R**), and the Kruskal-Wallis with the Dunn multiple comparisons test (**H**; α-SMA, Fibronectin, **K**, **L**; Ndufs1). The survival curve rate was analyzed by the Kaplan-Meier method and compared by the log-rank test in **A**. UK, UK5099 (a MPC1 inhibitor). GWx, GW604714x (an MPC1 inhibitor). *, vs sEVs or M3D-sEVs; #, vs sEVs+IgG, $P<0.05$. UK indicates UK5099; GWx, GW604714x. EF, ejection fraction; FS, fractional shortening; LV, left ventricular; FN, Fibronectin; Col, collagen I (COL1A1); and α-TUB, α-Tubulin.